Report

On the results of the research project

"Experiment COMET at J-PARC"

02-2-1144-2021/2022

1. Introduction

Despite successfully predicting and allowing understanding of phenomena in particle physics such as, most notably, the prediction and discovery of Higgs boson, the Standard Model (SM) cannot provide the ultimate description of nature: it lacks a viable dark matter candidate, offers no explanation to the observed matter-antimatter asymmetry of the Universe, and does not account for neutrino oscillation phenomena. There are also theoretical difficulties such as the hierarchy problem or the number of parameters in the SM, further suggesting the need for physics beyond the SM (BSM).

The observation of neutrino oscillations implies that neutrinos are massive, and that individual lepton flavors are not conserved. This contradicts the original SM formulation, in which neutrinos are massless by construction, and (accidental) symmetry leads to the conservation of total and individual lepton numbers. Such a departure from the SM paradigm also indicates that numerous other processes that are forbidden in the SM might indeed occur in nature. In particular, the violation of flavor conservation in the neutral lepton sector opens the door to the interesting possibility of charged-lepton flavor violation (CLFV). In addition to constituting a discovery of new physics, the observation of a CLFV transition could provide crucial information on the nature of the BSM physics at work. In the presence of new physics, one of the most interesting CLFV processes that can occur is the transition of a muon to an electron in the presence of a nucleus $\mu^- N \rightarrow e^- N$. The aim of the COMET experiment is to search for the $\mu^- N \rightarrow e^- N$ process.

COMET is an international collaboration and takes place at the Japan Proton Accelerator Research Complex (J-PARC) in Tokai, Japan. The experiment will be conducted in two phases. Phase-I will employ a simplified detector and will be used to investigate the beam and backgrounds whilst aiming at a sensitivity two orders of magnitude better than the current limit. Phase-II will use the information gained in Phase-I, a much more intense beam, and a more complex detection system to achieve a further two orders of magnitude of sensitivity. A third phase, PRISM (Phase-Rotated Intense Slow Muons), is being investigated and could potentially provide a further factor of 100 improvement.

2. The results obtained and the current status

The main contribution of JINR to COMET consists of participation in the production of three main detector systems: the electromagnetic calorimeter, the straw tracker, Cosmic Ray Veto (CRV) system, and includes variety of works on a simulation.

2.1. Electromagnetic Calorimeter

LYSO crystal parameters investigation

A significant disadvantage of the crystals based on the oxyorthosilicate of lutetium is a considerable variation of the light yield both over the length of an individual crystal (in the growing direction) and for different crystals. The light yield can be very different in length (decreases by 30-40% from the top to the bottom of the crystal). Thus, for homogeneous segmented ECAL, located in a magnetic field, the accuracy of measurement of deposited energy and energy resolution is influenced by:

- scintillation photons losses in the calorimeter cell (non-uniformity of light yield), depending on the track location in the crystal;
- electromagnetic shower losses in construction materials (reflective wrapping, etc.) and leakage outside the scintillator during passage of high energy particles through consecutive layers of the calorimeter.

The losses of the light yield along the crystal length, non-uniformity, energy resolution were experimentally measured. For this research LYSO crystals ($20 \times 20 \times 120$ mm^3), doped with 1.5% cerium of Saint-Gobain production, were used. In addition, a comparative estimate of the light yield for these crystals was obtained. The studies were performed by using a precision measuring setup, the results are published. It is established, that the energy resolution is on average equal to 8.9%, the coefficient of the non-uniformity is about 1.2 %/cm^{-1}.

Figures 1 (a) and (b) show the measured energy resolution and its non-uniformity of the light yield distribution along the crystal length measured at the ^{137}Cs (E = 661.65 keV).

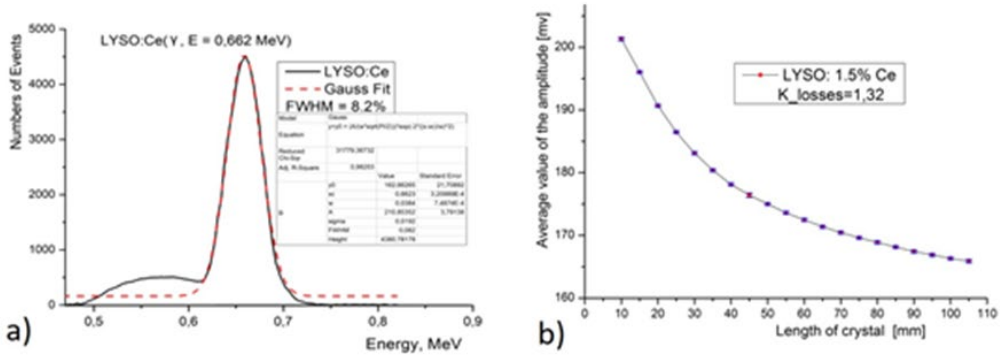

Fig. 1. Parameters of LYSO crystals: a) measured energy resolution; b) non-uniformity of the light yield distribution along the crystal length.

Figure 2 shows the light yield distribution measured in the middle of the length (L = 60 mm) under the same conditions for 49 crystals Saint-Gobain PreLude (TM)420 LYSO crystals manufactured at different times and chosen randomly.

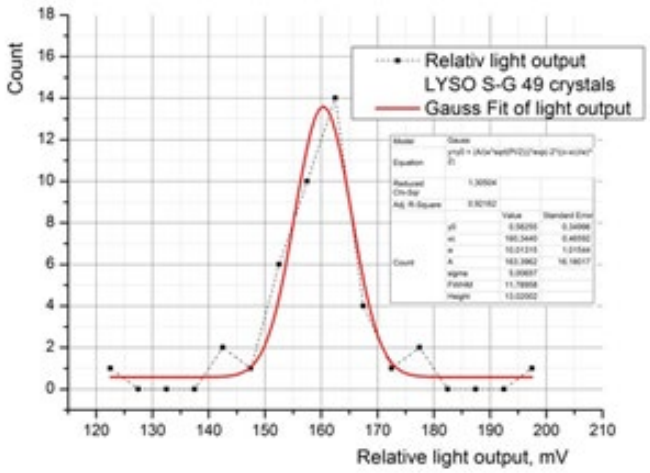

Fig. 2. Light yield distribution for 49 crystals.

The dependence of the light yield of the LYSO crystal on its orientation relative to the radiation source was also studied. Figure 3 shows a histogram of the change in light yield from the position of the ^{22}Na (1.271 MeV) radiation sources at the ends of the crystal in percent.

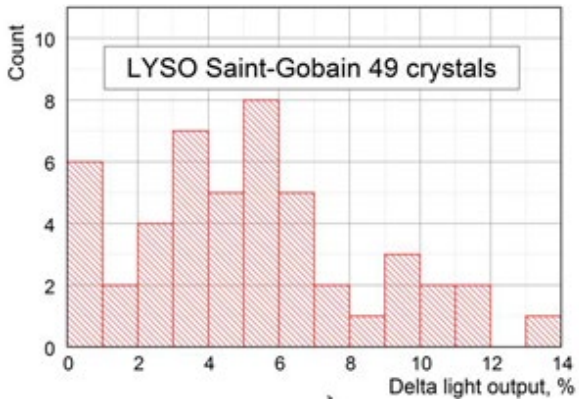

Fig. 3. Histogram of the change in light yield from the position of the radiation source.

Light collection

The non-uniformity of the light yield along the crystal length affects the accuracy of the measurement of the energy released in the calorimeter. In order to reduce the non-uniformity of the light yield, it is necessary to ensure a uniform collection of photons along the crystal length of the crystal. To reduce these losses, special light-reflective wraps are used.

For the development of techniques to improve the light collection we have investigated the light yield non-uniformity and energy resolution along the crystal length. It was obtained, that improvement of light collection could be achieved by use TEFLON tape as the diffusion-type layer (inner layer) and ESR as mirror type layer (outer layer).

Figure 4 (a) shows the light yield along the crystal length for a combined type of wrapper and for a LYSO crystal without a wrapper, and in Figure 4 (b) the corresponding energy resolution.

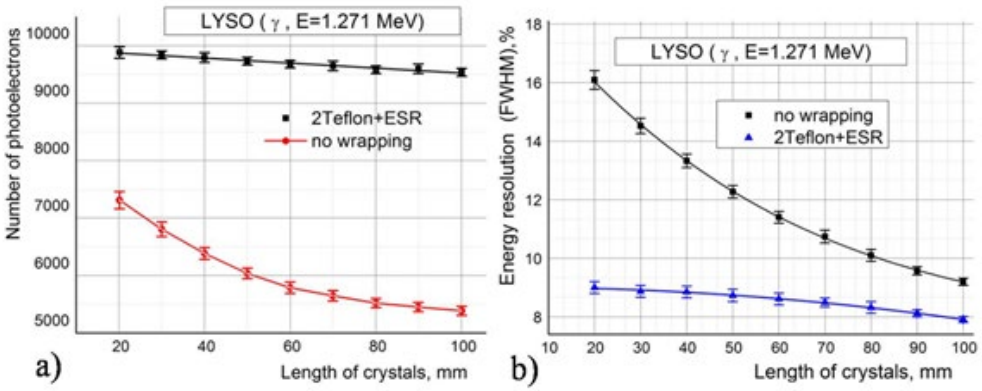

Fig. 4. Dependence of the light yield along the crystal length (a) and energy resolutions (b) for two cases: crystal without wrapping and with optimal wrapping.

Prototype measurement

The non-uniformity of the light yield along the crystal length will lead to an error in measuring the energy released in the calorimeter, especially when registering particles with curved tracks. Fig. 5 (a) shows the result of experimental verification of measurement error of the released energy in the prototype of the "Dubna" calorimeter at different angles of incidence of cosmic muons relative to the end surface of the calorimeter (Fig. 5 (b)). The prototype was made in the form of a matrix of 3x3 LYSO crystals (20×20×150 мм³), wrapped with a double layer of Teflon (AF1601, thickness 60 μm) and placed in an AL-Mylar module. For the readout of the signals were using the APD S8664-1010 (Hamamatsu). The error in measuring the energy for the 40 ° angle was 18.5%. Accounting for the measured calibration of the non-uniformity of the crystal improved the value of the energy released in the prototype by a factor of 2.8.

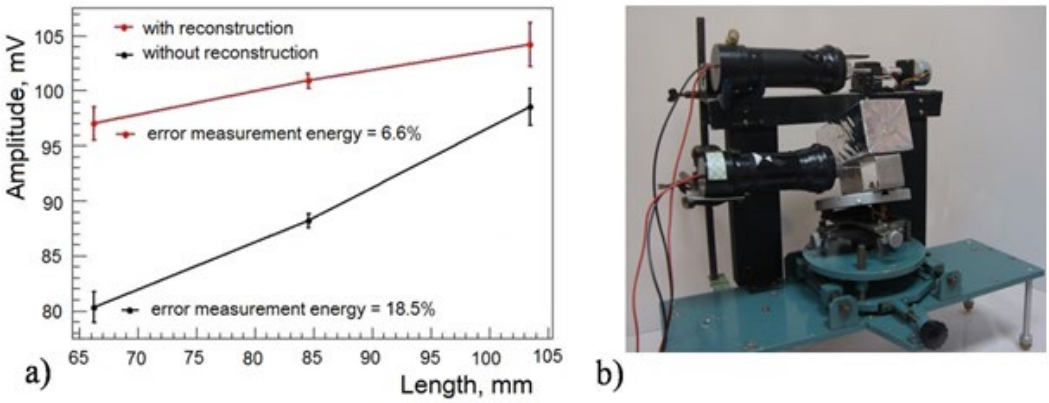

Fig. 5. a) Result of energy correction for muon; b) setup for measurements.

The LYSO crystal certification

The purpose of certification of the crystals LYSO(Ce) is to obtain the individual properties of each crystal. The measured properties are the relative light output, the attenuation of light in the crystal, and the non-uniformity of the light output. For these measurements, a stand was created, the scheme of which is shown in Fig. 6.

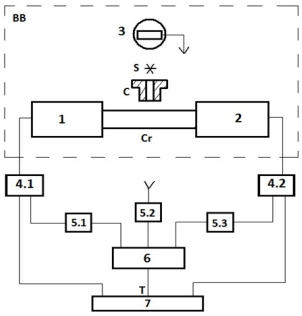

Fig. 6. Stand for certification of the LYSO(Ce) crystals.

The detecting part of the stand consists of the photomultipliers(1,2,3) and a precision mechanical bench with a source (S) displacement system placed in a black box (BB). Cr and S are a crystal and a collimator, respectively. The stand registration system consists of the linear gates (4), the discriminators (5), the coincidence circuits (6), and the digitizer V1742(7). All electronic modules from the company CAEN.

The measurements were carried out using a radioactive source Na-22. A typical spectrum obtained on a crystal is shown in Fig. 7.

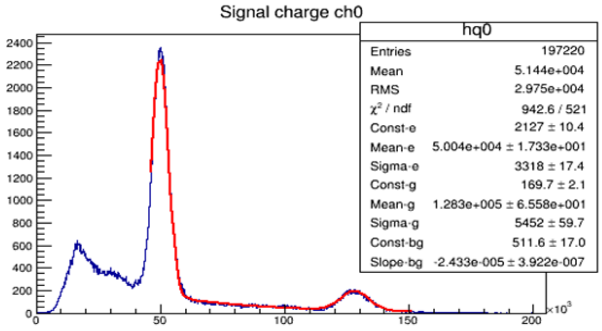

Fig. 7. The spectrum of Na-22 obtained on one of the crystals.

For each crystal, a set of such spectra was collected at different positions of the radioactive source above the crystal. Information on the light yield, attenuation coefficient, and the light output heterogeneity was extracted from these spectra.

In Fig. 8 and Fig. 9 the distributions of the light output and attenuation coefficient in one of the crystal batches are given.

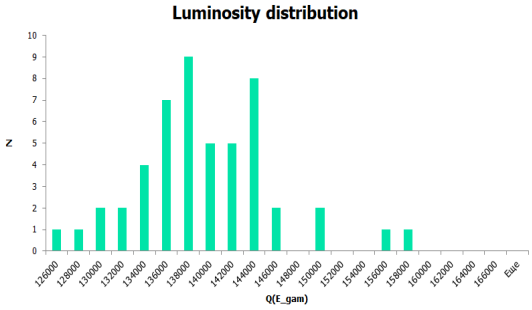

Fig. 8. A histogram of the brightness distribution.

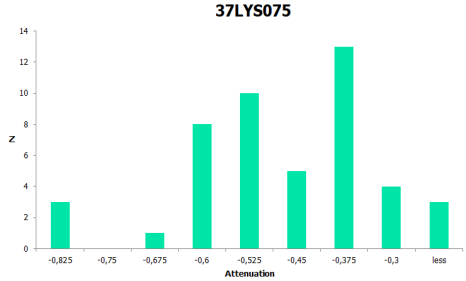

Fig. 9. A histogram of the distribution of attenuation coefficients for one of the batches.

So that, for each crystal we get a passport describing its main characteristics: the light attenuation and the energy resolution (Fig. 10). Currently, more than 200 crystals are measured.

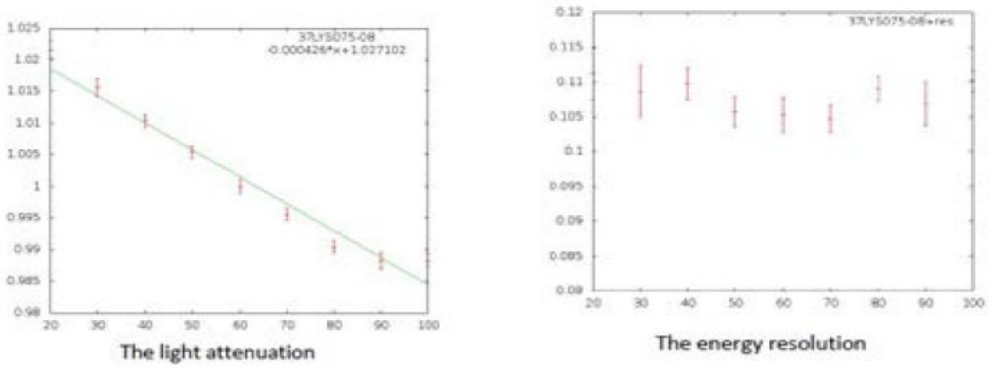

Fig. 10. The light attenuation and the energy resolution of the crystals.

Studies optical parameters of the new (engineering) LYSO crystals

Work on the study of the optical parameters (energy resolution, decay time, relative light yield, non-uniformity of the light distribution along the length) of a new (engineering) LYSO crystal from Saint-Gobain was continued. In addition, the study of the optical parameters of the Chinese crystal by JT Crystal Technology Co. Ltd.

It was obtained, that the light output of the LYSO engineering crystal is approximately 20% greater than previously produced crystals, but the energy resolution is practically the same. Decay time is slightly shorter. The non-uniformity of the light yield along the crystal length was studied (Fig. 11). The standard deviations of the light yield along the crystal length for a group of 10 samples relative to their average value is about 10 to 19% (Fig. 12).

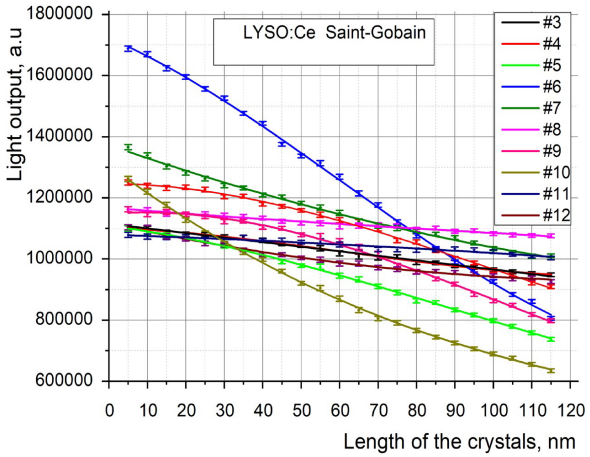

Fig. 11. Non-uniformity of LYSO crystal light yield along the crystal length.

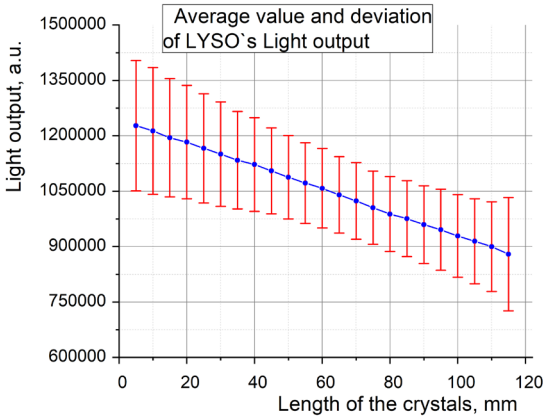

Fig. 12. Standard deviations of the light yield along the crystal length.

Measurements of the electromagnetic calorimeter prototype parameters of COMET experiment using cosmic muons

On the calorimeter prototype of the COMET experiment, performed on long LYSO: Ce crystals (Fig. 13) the non-uniformity of the detector response along the crystal length and at

angle of the 9 and 19 degrees relative to their end plane were measured using cosmic muons. An estimate of the energy resolution of the calorimeter of the COMET experiment was obtained.

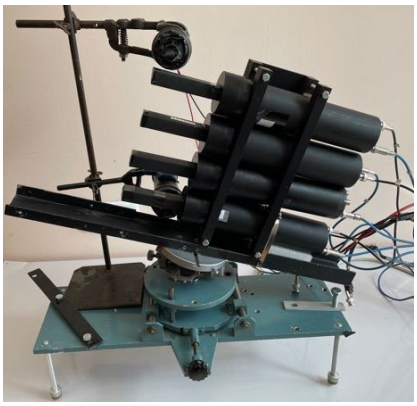

Fig. 13. COMET calorimeter prototype.

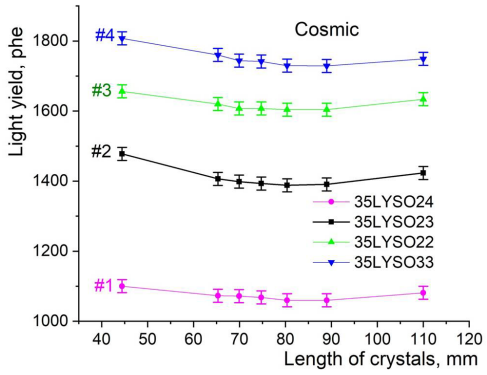

Fig. 14. Response non-uniformity of the calorimeter prototype along the crystal's length measured using cosmic muons.

Figure 14 presents the light yield non-uniformities (responses) along the scintillator length measured using cosmic muons. Figure 15 (a) presents the scintillators responses non-uniformity of the calorimeter prototype measured using cosmic muons for the incidence angles of the 9 and 19° of the cosmic muons relative to the scintillators end surfaces. From the measurement results, it follows that the non-uniformity of the calorimeter prototype response increases with the increase angle respect to the value at zero angle (Fig. 15 (a)). Figure 15 (b) presents the mean and non-uniformity of response depending on the incidence angle of cosmic muons for each calorimeter prototype scintillator.

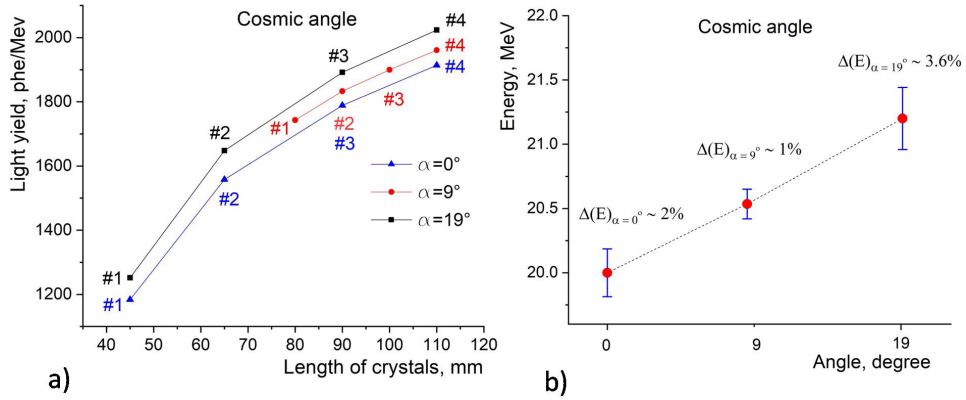

Fig. 15. Non-uniformity of the detector response for angles 19° and 9° measured using cosmic muons a) distributions of the non-uniformity of the scintillators responses of the calorimeter prototype over the angle; b) mean and non-uniformity of the detector response over angle.

As a result of measurements, the following results were obtained: 1) light yield non-uniformity along the length, measured at the source and at the cosmic muons, have the same distribution pattern; 2) energy resolution of the calorimeter prototype at the angle of 19° is ~ 6%. Measurements performed showed that it is necessary to take into account the

scintillators responses non-uniformity when creating a calorimeter with the required resolution on LYSO crystals in the COMET experiment.

According to the results, a comparison of the optical parameters of LYSO crystals from JT Crystal Technology Co. Ltd. and Saint-Gobain published an article (V. Kalinnikov, E. Velicheva, Yusuke Uozumi, Comparison of the Scintillation Properties of Long LYSO:Ce Crystals from Different Manufacturers. //Physics of Particles and Nuclei Letters, 2021, Vol. 18, No. 4, pp. 457–468).

The study and comparison of the optical parameters (relative light yield, energy resolution, decay time) of LYSO:Ce and LYSO:Ce,Ca (double doped) crystals from Saint-Gobain (France) was carried out. We studied 8 samples of each type of crystals with a size of 20×20×120 mm^3 wrapped with a Teflon reflective tape 65 μm thick (TEFLON AF1601). The crystals were measured on a precision measuring setup with use an H1949-51 PMT and a 5 GHz, 3 VME VX1742B digitizer. The ^{22}Na radiation source in the collimator was located at a distance of 12 mm above the crystal surface, and measurements were carried out with a step of 5 mm. Fig. 16 shown the scintillators responses of two groups of the crystals: LYSO:Ce (Fig. 16 (a)) and LYSO:Ce,Ca (Fig. 16 (b)). The following results were obtained: 1) the mean value of the scintillators responses non-uniformity for LYSO:Ce crystals is ~ 4.6%, and for LYSO:Ce,Ca is ~.1.1%; 2) for the entire group of LYSO:Ce crystals, energy resolution scatter at the middle of the length is ± 0.21%, and for LYSO:Ce:Ca is ± 0.19%. The light yield scatter near the crystals end surface is ~26 and 20% for LYSO:Ce and LYSO:Ce,Ca, respectively. The decay time of LYSO:Ce crystals is 8 ns longer than that of LYSO:Ce,Ca.

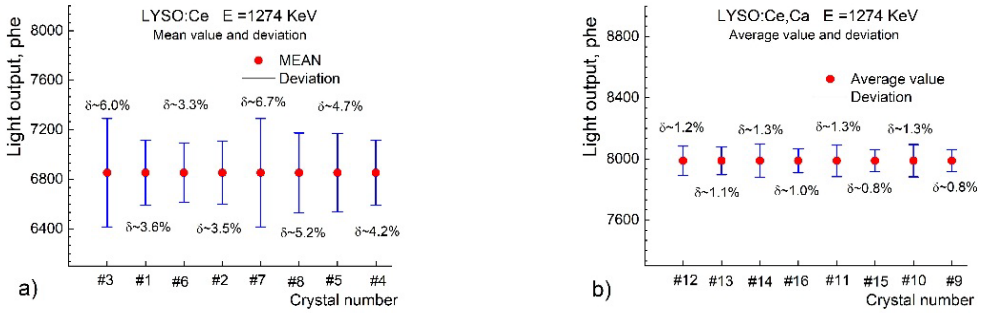

Fig. 16. Mean values and scintillator responses non-uniformity for each sample: a) LYSO:Ce crystals; b) LYSO:Ce,Ca crystals.

Based on the results of the study, an article was written, which was sent to the journal "Physics of Particles and Nuclei Letters" and is at the stage of review. In addition, an article was published in 2022: V. Kalinnikov, E. Velicheva, Measurements of the electromagnetic calorimeter prototype parameters of COMET experiment using cosmic muons // Physics of Particles and Nuclei Letters, 2022, Vol. 19, No. 3, pp. 225–234., 2022.

The JINR physicists participated in assembling of the prototype, beam measurements and fulfilled independent analysis of the beam test results. Following these investigations, the collaboration has selected the LYSO crystal as one to be used in the calorimeter.

2.2. Straw tracker system

Straw module design

Straw tracker system consists of five connected modules. First version of straw module has been designed supposing that working gas mixture flowing through the straws also serves as a cooling agent for ROESTI boards placed along rounded surface next to straws but tests with cooling the boards showed that level of working gas flow cannot provide needed cooling. As a consequence, new design with two separate gas flows is needed. Such a design is being developed and design of the support structure is now completed.

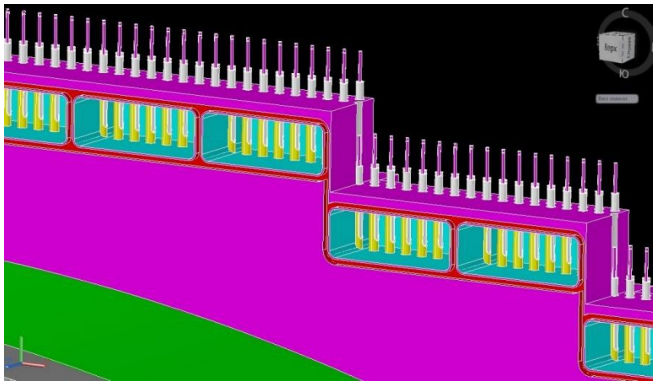

Fig. 17. Design of support structure.

One may see from the Fig. 17 that gas flow for all the straws goes through the special caverns made in the body in which the straws are fixed. Each straw is ended with end-plug having small hole for the input of gas. The dimension of each cavern along the straw allows the hole to be located inside the cavern. Thus, the gas coming inside the cavern through the gas connector on the tightening lid goes inside the straw through the end-plug hole. At the same time, electrical part on the end-plug is outside the cavern thus facilitating fixing the electrical connector.

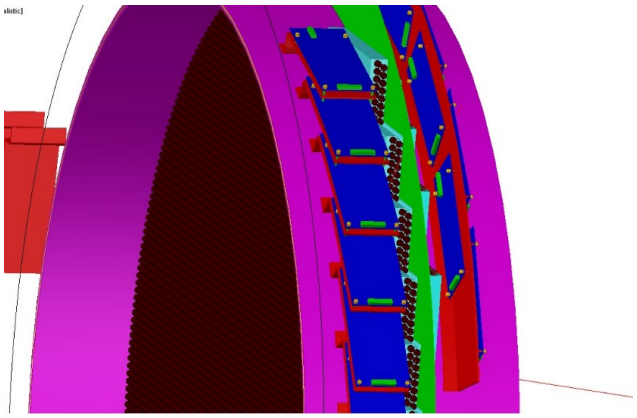

Fig. 18. Schematic view of the ROESTI boards.

Schematic view of the ROESTI boards located along the rounded surface of the support structure is shown on the Fig. 18. For their cooling rather strong flow of the gas is needed. Now the developed structure allows for two independent flows.

One more challenge for the straw module production is very small gap between adjacent holes for fixing straws equal to 0.5 mm. Important after a lot of tries one succeeded to provide

a deep drilling of the holes keeping the gap of 0.5 mm along the hole. Design of the straw tracker module support structure is completed, and its production is started. The support structure has more than 2000 holes of diameter of 5mm with a pitch of 0.5mm. Functional and constructive update of the 16-channel readout board ROESTI is in progress.

Straw tubes checking in Japan

Within the COMET Phase-I, 2700 full-size (1.2 m and 1.6 m length) straw tubes have been produced, after testing and checking according to quality standard all tubes were sent to Japan at KEK and from there to J-PARC (Fig. 19). Due to the specific properties of Mylar and 20 μm wall thickness of straw tubes, long-term keeping requires constant monitoring and controlling of storage condition (quality control procedures must be carried out every 6 months).

Fig. 19. J-PARC Clean room in experimental hall.

Experience has shown that in order to maintain normal physical storage conditions and ensure safe transportation from JINR to the KEK, the tubes must be under pressure (Fig. 20). This also makes it possible to observe their behavior under similar conditions, like in a detector. For this, the tubes were prepared with the following conditions: initial gas pressure ~2.5 bar.

Fig. 20. Left: Construction of ready straw tube; Right: Specific design of transport pads.

October 2017, at the J-PARC started a regular checking process of the straw tube conditions (Fig. 21). Some of them successfully passed all checks; other tubes were refined in April 2018. At this moment, all tubes are sorted, tested and ready for assembly in the straw tracker detector modules.

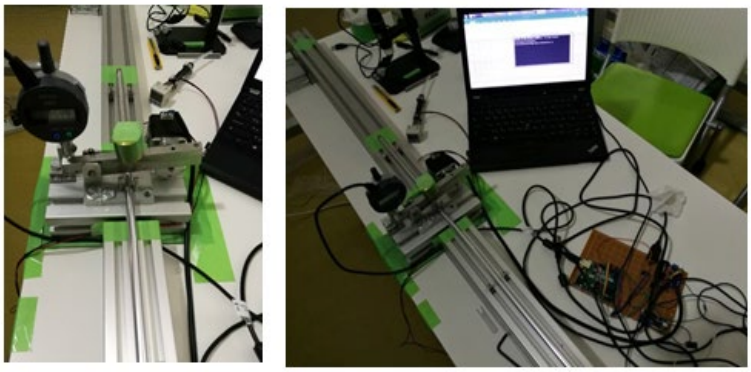

Fig. 21. Pressure measure device: designed and developed at JINR.

By results, the pressure in the tubes dropped about 0.7 bar during 2 years of storage (Fig. 22). This is an excellent result for 20 μm wall thickness straw tubes. One of the causes of gas leakage is micro-shells between the wall of the straw and the endplugs, as well as the rubber ring between the endplugs and the gas blockers. The following figure shows the results of pressure measurements.

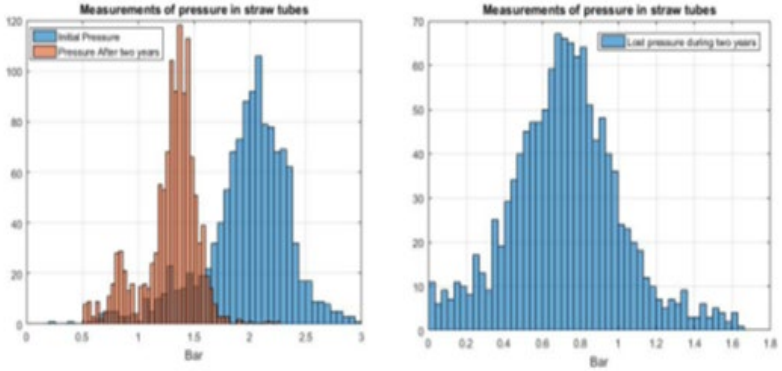

Fig. 22. Left: Initial pressure in the tubes and after two years. Right: Gas lost in the two years.

In conclusion, the first measurements were done successfully, all safety conditions for long-term keeping are restored and straw tubes are ready for assembling in detector modules and for afterward tests.

The manufacturing area for straw-tube R&D and production at DLNP, JINR

Over the past years, a method of using ultrasonic welding technologies of straw production, which does not require multiple over-woven layers, has been developed by the JINR group for the NA62 experiment at CERN. In this method, a single layer is rolled and attached to itself in a straight line without using glue. Later by JINR-COMET group, this method and equipment were obtained in order to be improved and 2700 units of straw tubes were made for Phase-I with thinner wall 20 μm and 9.8 mm in diameter. Many stress and long-term holding tests showed their reliability for using in vacuum conditions (Table 1).

Unit	Diameter	Working pressure	Max pressure
2700	9.8 mm	1 bar	6 bar

Table 1. Some results for straw tubes with thickness of 20 μm and a diameter of 9.8 mm.

In order to achieve the ambitious goal of the COMET experiment (Phase-II) mu-e conversion measurements at level 10^{-17}, one of the main and crucial parts of the detector systems is a straw tube tracker. To achieve a high momentum resolution better than 2 % for 100 MeV/c electron, a very light-material for straw tubes is needed.

According to the main requirements of COMET project in Phase-II must be used straw tubes with 12 μm thick walls and 5 mm in diameter. Thin walls of straw tubes is a crucial moment for tracker detector in order to reduce multiple scattering. In order to achieve the mentioned goals and make straws with the required parameters, the JINR-COMET group created a special laboratory to develop and produce unique straw tubes with new parameters using ultrasonic welding technology. The purpose of this laboratory is to manufacture and test straws with a wall thickness of 12 μm and a diameter of 5 mm. For this we created:

- A clean room of class 5, providing controlled parameters for the production, testing and storage of straw tubes.
- The design of the area provides pure air in the full volume of two rooms and controlled humidity and temperature. The surface of the walls and roof of the rooms covered with special electrostatic (repulsive) paint. New mechanical management device is engineering for forming 5mm straw tubes.
- A special installation with a high-precision positioning system for welding pipes from straw using an ultrasonic generator and accurately drawing a line of straw that can be moved up to a distance of 2 m.
- Equipment for automatic control of manufacturing process has been created. At this time, adjusting of automation system is in progress.

After configuring the welding machine and the first studies, the first welded pipes of straw with a length of 1400 mm, a thickness of 12 μm and a diameter of 5-10 mm were obtained (Fig. 23).

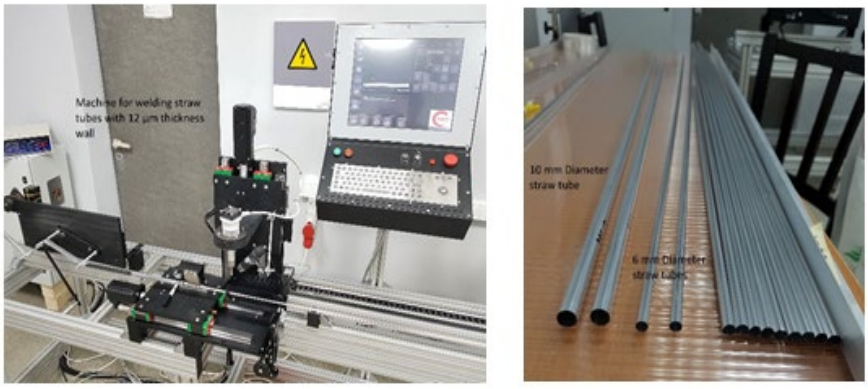

Fig. 23. Left: Welding machine; Right: 9.8 mm and 6 mm straw tubes.

Development and creation Ultrathin 12 μm Thick Straw Tubes for the Tracking Detector of the COMET experiment

New extremely thin-wall straw tubes have the ability to successfully operate in a vacuum and in a 1 Tesla magnetic field. These straw tubes are made by using an ultrasonic welding technology. In this way, the newly developed straw tubes with 12 μm ultra-thin walls can

guarantee a minimal multiple scattering effect, have a high resistance to gas leakage, provide a precise detection of a particle and have a reliable operation.

The main part of this technology is an ultrasonic welding process, which uses a special generator constructed according to pre-settled parameters. The straw tube produced by this method provides elasticity and reliability through its whole length. The described process is shown on Fig. 24.

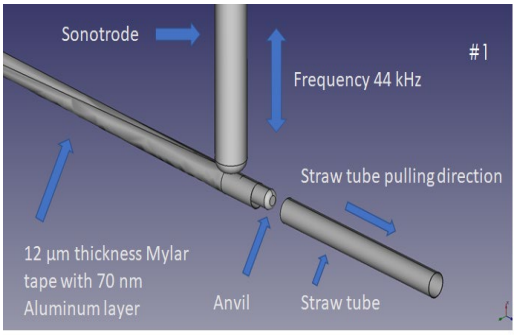

Fig. 24. Straw tube manufacturing process using ultrasonic welding technology.

The reliability of the tube is controlled by the configuration of the appropriate parameters during the welding process. It totally affects the ability of the straw to keep its elastic properties along the cylinder. For the sake of reliability and quality control, the welding process needs a special investigation. Each tube passes through an optical visual inspection and a variety of other tests. The structure of the seam is shown in Fig. 25.

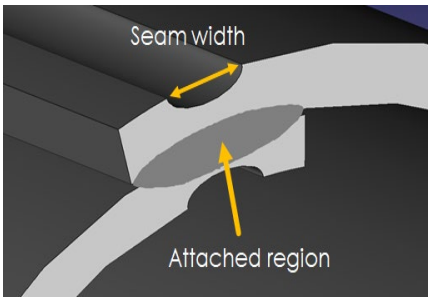

Fig. 25. Seam structure.

New design straw tubes with 12-micron wall-thickness and 4.97 mm diameter were successfully manufactured for the purposes of the COMET experiment. The new generation of straw tubes were tested on the next parameters: cylindrical shape uniformity over pressurizing, seam strength, diameter stability and gas leakage. They showed excellent characteristics and working properties.

The uniformity of the cylinder diameter is a crucial point for the straw tubes. Straw tubes must pass a cylindrical shape uniformity test in order to be approved for exploitation. This parameter is controlled by a special optical device. The straw tube is placed perpendicularly to a laser beam and its diameter is measured with accuracy of 0.1 μm. The straw tube is scanned at 1-2 bar pressure. This method of testing is used to assess cylinder diameter uniformity at different points.

The graph on Fig. 26 shows the dependence between the straw diameter and the testing pressure. The blue line shows the deviation from the mean diameter at 1 bar pressure. The

purple line represents the deviation from the mean diameter at 2 bar pressure. The results show that the increase of pressure leads to an increase of diameter deviation.

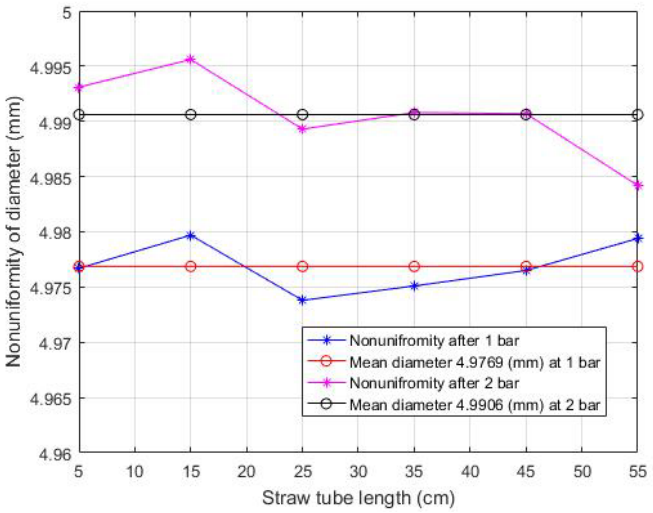

Fig. 26. Dependence of straw tube diameter non-uniformity on applied pressure.

Straw tube samples are also studied by pressure stress tests. The newly developed 12 μm straws show the ability to hold absolute ~4 bar over pressurization without any visible deformation in their shape. The aforementioned stress tests are performed in order to check the quality of the straw tube manufacturing process, the strength and reliability of the welded region.

The tested samples show excellent seam strength, which guarantees the long operational life of straws. The quick tests on gas leakage also show satisfactory results and minimal leakage, which doesn't affect their working ability in vacuum. Further and more detailed studies and tests will be performed in order to improve the straw tube parameters.

For the ambitious goal of the COMET experiment new extremely thin 12 μm straw tubes were developed (Fig. 27). They can provide a high momentum resolution and operate reliably in conditions of 10^{-6} mbar vacuum.

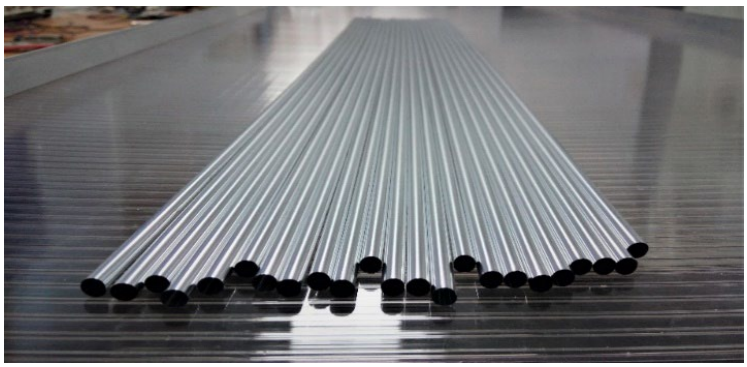

Fig. 27. New straw tube with 5 mm diameter for JINR detector prototype.

For the production of tubes with such small diameter, new methods of quality control were developed. Using this new methodology straw tubes were scanned along the axes for the monitoring of the uniformity of diameter with the precision of 0.1 μm. Scan data shows the maximum deviation of 15 μm from the average diameter values (Fig. 28).

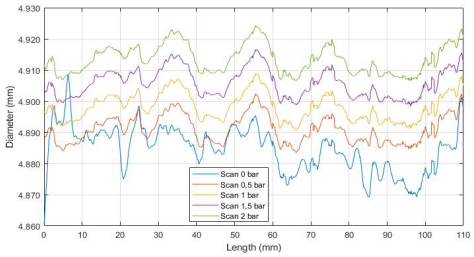

Fig. 28. Scan of tube dimeter along its axes with different pressure.

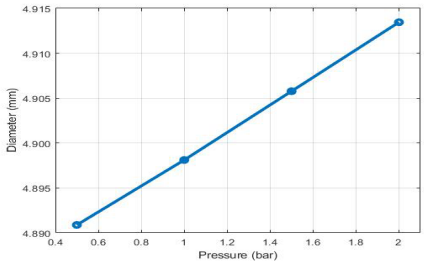

Fig. 29. Dependency of tube diameter from inner pressure.

Additional measurements intended to the study of dependence of the tube diameter from the inner pressure were performed via changing the pressure with step of 0.5 bar in the interval from 0 to 2 bar. Measurements showed that as result of growing the pressure by every 1 bar the diameter of tube changes for about 15 μm. This are excellent feature for such thin-walled tube and important characteristic for a proper operation of the detector.

At this moment a 100 pc. of 70 cm straw tubes were produced for the tracking detector prototype which is currently under development at JINR.

The results fully satisfy the requirements of the COMET experiment. In the future, a more thorough study of the properties of straw tubes and the development of tests for quality control is planned. After the completion of all research work, the mass production of straw tubes for the COMET Phase-II experiment will begin.

In conclusion, the achieved parameters of the new straw tubes give them a great advantage and opportunity to be used in all current world leading experiments with tracking detector systems.

1Chanel Test Setup

Main issues:

1. Choose the optimal wire diameter. Due to the fact that the diameter of the tube is reduced by half in COMET Phase II.

There is a possibility that the wire with a thickness of 25 microns or less will not have enough of the allowable tension in order to avoid the effect of "sticking" of the anode wire to the walls. For example, in ATLAS TRT straw 4mm, 31 μm wires were used with wire support.

2. Determine the straw pretension WITHOUT.

There is a possibility without excess pressure, when the straw is pulled, the central part can take the form of an elapse. In this connection, the breakdown voltage will be lower than the voltage required for the normal operation of the tube. This must be considered when testing the station outside of vacuum. Working pressure of the gas in the detector is one excess atmosphere.

3. Assemble the working channel and test it on the Fe55 source
4. Testing a new type of end plugs produced by SLM (Selective Laser Sintering) 3D printer of nylon.

Based on the above, assemble a mini station prototype (64ch) based on 5mm straw tubes with 50 cm length for the COMET experiment Phase II, and testing on the electron beam.

Below is the main view of the 1Chanel Test Setup (5mm straw assembly), the external view of the test bench and general connection diagram.

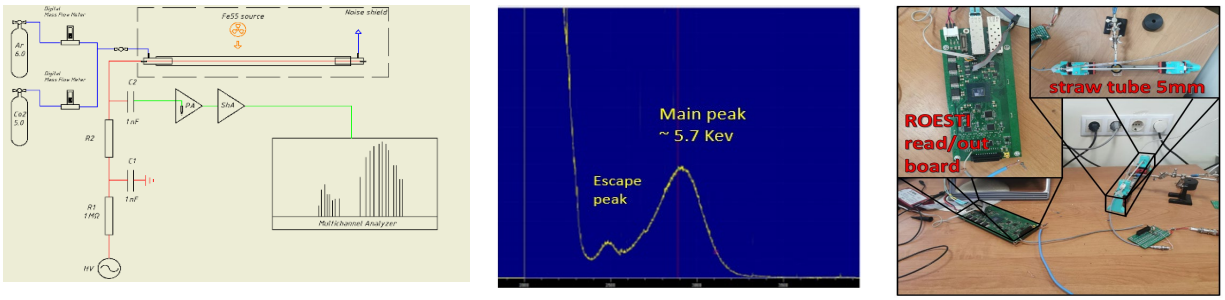

Fig. 30. The main view of the gas supply system. Fe55 spectrum.

Measurements showed good separation of signal peaks from noise (see Fig. 30).

As measurements have shown, when the tube is stretched about 50 grams, the tube is deformed due to the thin wall, which leads to a decrease in the gap between the wire and the cathode, and eventually the tube begins to pierce. The study of the dependence of the critical diameter of tubes depending on pressure and tension was carried out on a test bench (see Fig. 31).

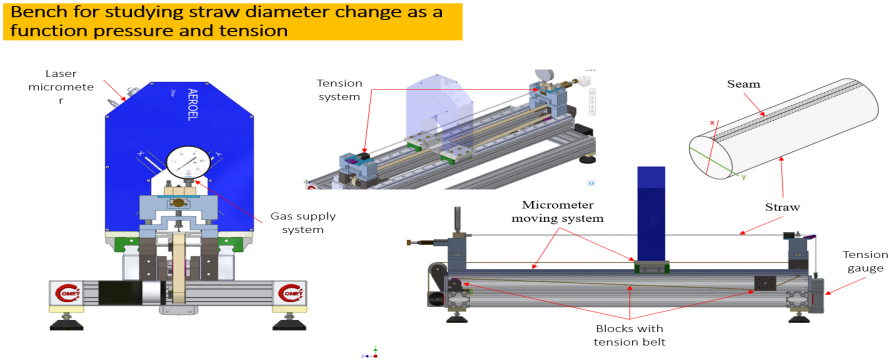

Fig. 31. The main view of the test bench.

Main results:

1. Measurements showed the effectiveness of 5mm straw and 50μm wire. Assembly of the channel with smaller diameter wire in the process of development.
2. Assembled a 5mm frame for a mini prototype station straw tracker of the COMET experiment for 64 channels.
3. Studying the tension relaxation in the process.
4. Tested 4 ROESTI electronics boards.

The JINR physicists will be involved in assembling and tests of the full-scale straw tracker, first for Phase-I and then R&D works for straw tracker for Phase-II of COMET.

The properties of straws

A bench with termostabilization system for measuring of properties of the straws

In order to ensure straw detector's high coordinate accuracy, in addition to the precise positioning of the wire inside the tube and the tubes themselves in the detector's modules the material from which straws are made is required to maintain its basic physical properties over

time. As well as the material is required to be uniform throughout the length of the tube. The most important straw material's physical properties are: the area of elastic deformation, the value of the elastic modulus, which characterizes the straw strength depends, the relaxation rate of tension. The Poisson's ratio allows determining the impact of pressure drop on the straw wall on its tension. These parameters largely influence the detector design's choice and the straw lifetime in the experiment. The study of straw properties' changes in the time, as well as estimation of straw lifetime in the detector, are an important task.

Based on the above, the following work was performed:

1. A bench with termostabilization system for measuring of properties of the straws (Fig. 32) was developed and established.

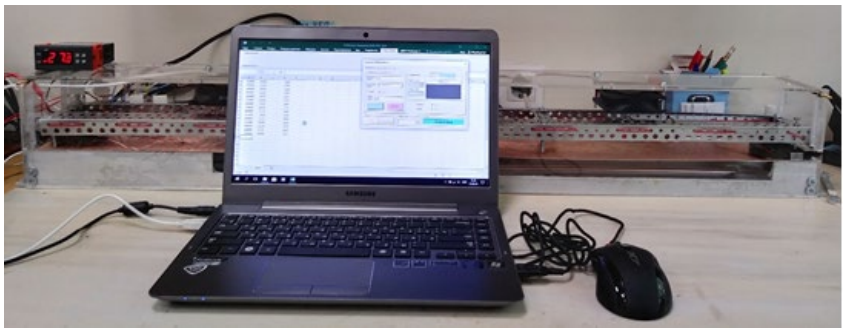

Fig. 32. Developed stand's general view.

2. The following mechanical properties of the 9.8 mm straws have been measured:

a) the range of elastic deformation of the straw (Fig. 33);

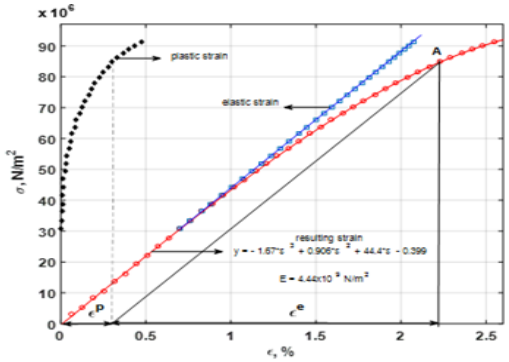

Fig. 33. Measurement of the elastic and plastic deformation's area.

b) the influence of temperature and the dependence of the elastic properties of the straw on its thickness (Fig. 34);

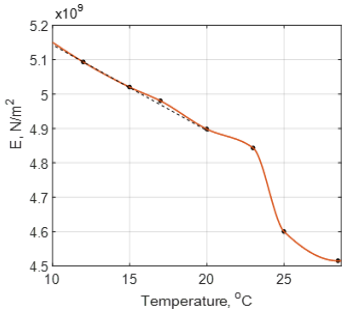

Fig. 34. Measurement of the influence of temperature and the dependence of the elastic properties of the straw on its thickness.

c) the effect of pressure drop of the straw's internal pressure on its tension, which causes an increase in tension by 480 gf/atm;

d) preliminary data on the stress relaxation of the straw were obtained (Fig. 35) on which the lifetime of the straws as a part of the detector in the experiment was estimated.

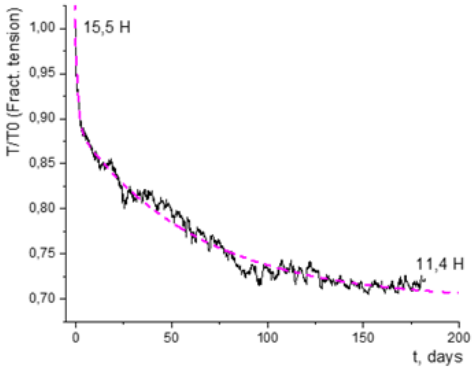

Fig. 35. Stress relaxation on time.

The results of measurements are being prepared for publication. An application for the patent for the invention on the bench with term stabilization system for measuring of properties of the straws is also being prepared.

In 2019, a stand was created and the properties of 20 microns of straw with a diameter of 9.8 mm were studied. The relaxation of straw tension in time is investigated. The straw tension of 1.3 kg is selected, which ensures the detector operability for 9 years.

Stand for studying the diameter of the straw depending on various parameters: tension, pressure

In the case of mass production of straw, quality control is required, with the entry of parameters into the database. For this, a bench (Fig. 36) was developed that allows you to measure the diameter of the straw depending on various parameters: tension, pressure. And also evaluate the deviation of the straw from the cylindrical shape. This bench allows us to measure straws up to 800mm in length with the ability to scale to measure any length of action. Working pressure range in the tube (0, 0.1, 0.2… 2.5 bar). The accuracy of the micrometer movement along the tube axis is up to 1 mm.

Fig. 36. Stand for studying the characteristics of straw tubes.

The simulation of straws

Isochrones

There were built isochrones for 105 MeV/c electron in different gas mixtures (Ar-CO_2 (90%-10%, 80%-20%, 70%-30%, 60%-40%, 50%-50%, Ar-C_2H_6 (50%-50%)) and different voltages (1500 V - 2000 V), in the presence of magnetic field (1 Tesla) and without it in the Fortran version of Garfield. These simulations were done for a tube with diameter of 10 mm and a wire with diameter of 25 microns. In other words, a source file for different cases was written to run them under Garfield. Two types of graphs were obtained: flat and three-dimensional (Fig. 37).

Files with transport parameters for gas mixtures were provided, some of them were excluding the magnetic field, another part of them were taking into account the magnetic field (1 Tesla), and different angles (from 0 to 90 degrees in increments of 10 degrees) between the vectors of electric E and magnetic B fields. Isochrones were built for several gas files for the gas mixture Ar-C_2H_6 (50%-50%) with certain specified angles (0, 30, 60 and 90 degrees), for vertical and horizontal positioning of tubes (Fig. 38).

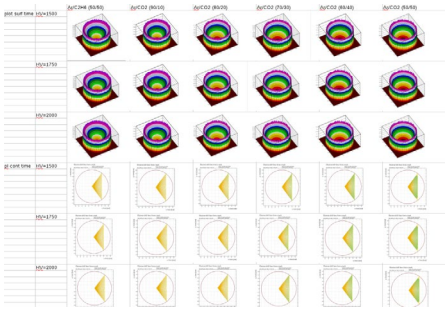

Fig. 37. Isochrones for 105 MeV/c electron in different gas mixtures, without magnetic field.

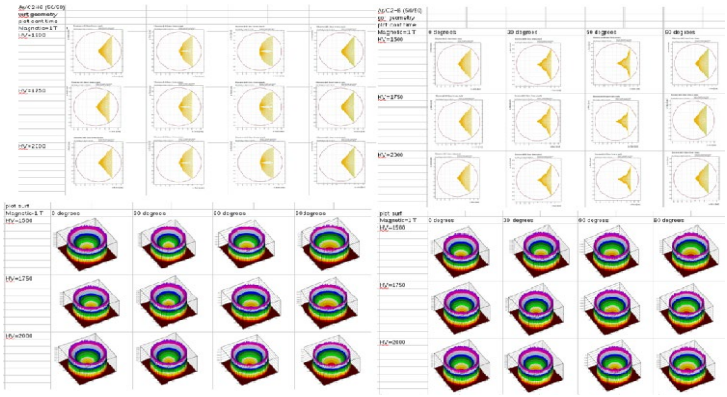

Fig. 38. Isochrones for Ar-C_2H_6 (50%-50%) with magnetic field 1 Tesla.

To check the obtained graphs, x(t) plots for the corresponding gas mixtures were built (Fig. 39). The x(t) plot shows the relation between the position of a track and the drift time.

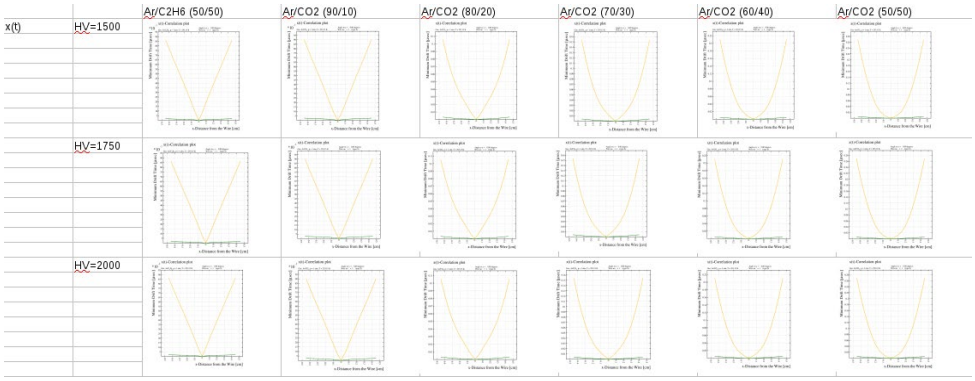

Fig. 39. X(t) for the all corresponding gas mixtures.

Study of gas mixtures of candidates for use in the Phase-I COMET experiment

Selectable gas mixtures must meet the following criteria:

1. Ensuring performance at low electric field strengths.

2. High gas gain. It is necessary for the efficient registration of particles and etc.

Gas mixtures were studied: Ar-C_2H_6 (in the proportion of 50% -50%) and Ar-CO_2 (in the proportions of 50% -50%, 60% -40%, 70% -30%, 80% -20%, 90% -10%).

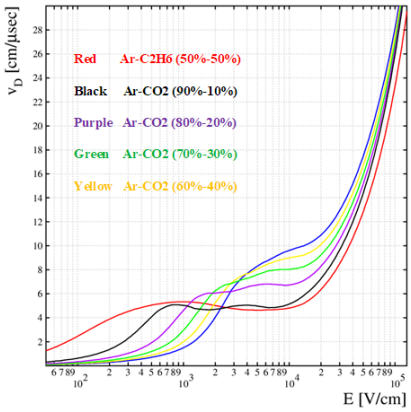

Fig. 40. The dependence of the drift velocity of electrons on the magnitude of the electric field strength for various gases. T = 273.15 K, p = 1 atm.

Drift velocity

As follows from Fig. 40. The drift velocity of electrons for the Ar-C_2H_6 gas mixture (50% -50%) has a wide plateau in the range of 1 kV/cm - 10 kV/cm and is 5 cm/μc. As the concentration of argon in an Ar-CO_2 mixture increases, there is a tendency to form a plateau and increase its width.

Consider the influence of the magnetic field and the angle between the electric and magnetic fields on the drift velocity. See Fig. 41, Fig. 42.

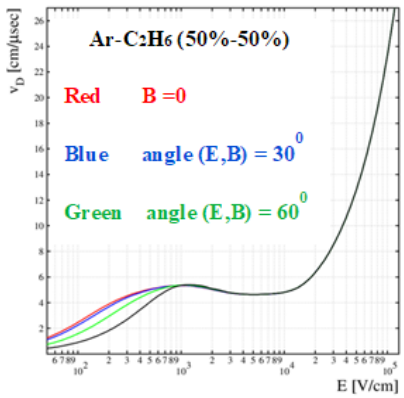

Fig. 41. Dependence of the drift velocity of electrons in the Ar-C2H6 gas mixture (50%-50%; T = 273.15 K, p = 1 atm) on the magnitude of the electric field (Red line). Accounting for a uniform magnetic field of 1 T at various angles (E, B) = 30°, 60°, 90° (blue, green, black line).

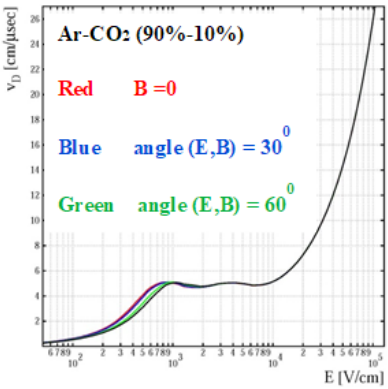

Fig. 42. Dependence of the drift velocity of electrons in the Ar-CO2 gas mixture (90%-10%; T = 273.15 K, p = 1 atm) on the magnitude of the electric field (Red Line). Accounting for a uniform magnetic field of 1 T at various angles (E, B) = 30°, 60°, 90° (blue, green, black line).

The intensity of the electric field inside the straw tube varies from about 700 V/cm to 270000 V/cm, with such electric fields we have no influence of the magnetic field on the magnitude of the drift velocity. The effect of the magnetic field on diffusion will be more significant.

Diffusion

Comparison of total diffusions for all considered gas mixtures in the limiting case, when the angle between the magnetic and electric field 90° is given in Fig. 43.

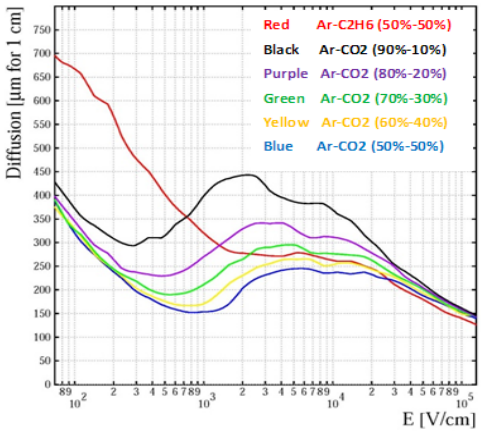

Fig. 43. The dependence of diffusion D in gas mixtures at an angle (E, B) = 90°

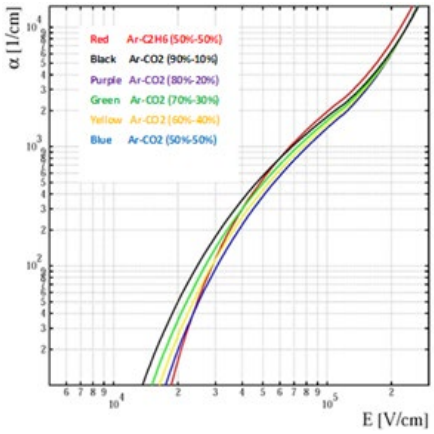

Fig. 44. The dependence of the first Townsend coefficient on the magnitude of the electric field strength for various gases. T = 273.15 K, p = 1 atm.

Townsend coefficients

As follows from Fig. 44, for large electric fields (near the anode wire), the first Townsend coefficient is greater in the case of the Ar-C_2H_6 gas mixture this will lead to a stronger gas amplification compared to Ar-CO_2.

Simulation of the straw tube response to an electron pulse of 105 MeV/c for Phase–I

To determine the mean values (Table 2), the obtained distributions (Fig. 45, Fig. 46), were approximated in the ROOT package using a lognormal distribution.

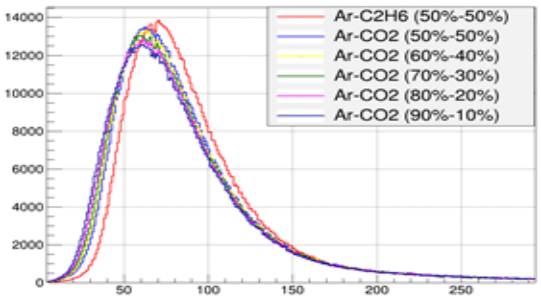

Fig. 45. The number of ionization clusters per unit path length for different gas mixtures. Oy - the number of events.

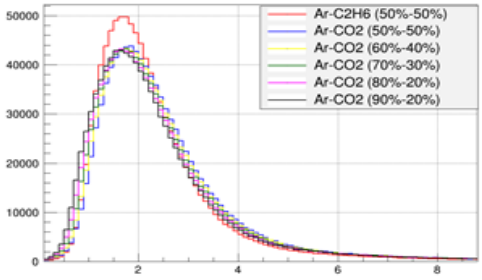

Fig. 46. Ionization loss per unit path length for various gas mixtures. Oy - the number of events.

Table 2. The number of ionization clusters, and ionization losses per unit length of the track in various gas mixtures.

Gas mixture	dE/dx, [keV/cm]	Ne, cm^{-1}
Ar-C_2H_6 (50-50)	1,66	69,06
Ar-CO_2 (50-50)	1,77	63,10
Ar-CO_2 (60-40)	1,74	62,37
Ar-CO_2 (70-30)	1,71	61,73
Ar-CO_2 (80-20)	1,67	61,24
Ar-CO_2 (90-10)	1,65	60,71

The effect of the seam on the collection of primary ionization

For the production of straw-tubes, the ultrasonic welding method is used. With this method, the tube has a non-conductive layer of surface along the wire named «seam». It is necessary to estimate the effect of the seam on the electric field inside the straw tube. At the beginning, the weld effect is evaluated for a tube with a diameter of 9.48 mm for Phase I. In the case Phase II the diameter of the straw tube is 5 mm, whereas the width of the seam is about 500 micron which is one- thirtieth of the circumference of the tube.

To solve this problem, an algorithm was developed for finding the distribution of charges on the surface of the straw tube.

The results of the distributions for the case without a seam and with a seam are shown in the Fig. 47 and Fig. 48.

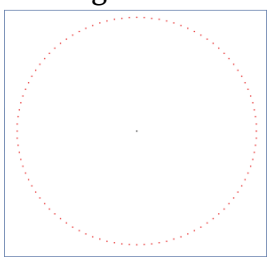

Fig. 47. Stationary state of charge. Straw - tube without seam.

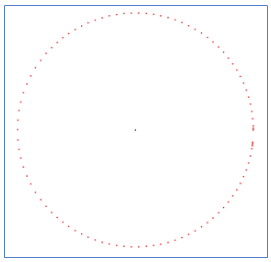

Fig. 48. Stationary state of charge. Straw - tube with seam.

Nonlinearity of the charge distribution leads to an asymmetric distribution of the electric field inside the straw tube. The Fig. 49 shows the value of electric field strength.

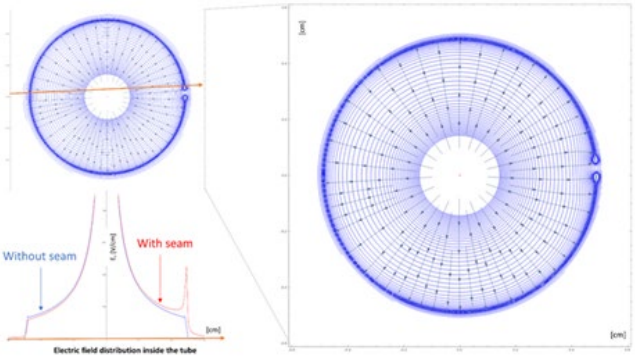

Fig. 49. The distribution of the electric field inside the straw tube with/without seam. Garfield++.

The main task was to estimate the effect of a distorted electric field on the collection of ionization at the anode and the XT relation. Comparison of XT relation when the straw tube has a seam is shown in the Fig. 50.

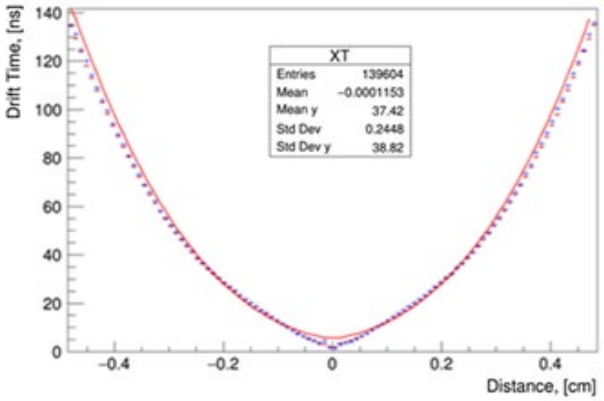

Fig. 50. XT relation. UserField with a seam (+), Analytic field without a seam (- - -), Experiment (-). Garfield++.

The presence of a seam does not effect on XT relation. To determine the degree of influence of the seam on the collection of ionization electrons at the anode. Let us take the selected direction of the passing electron see Fig. 51.

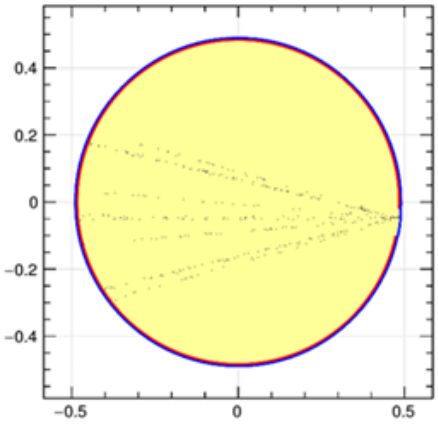

Fig. 51. The selected direction of the passing electron. Garfield++.

As we see from the graph presented below, we have no loss of primary ionization electron collection at the anode (Fig. 52):

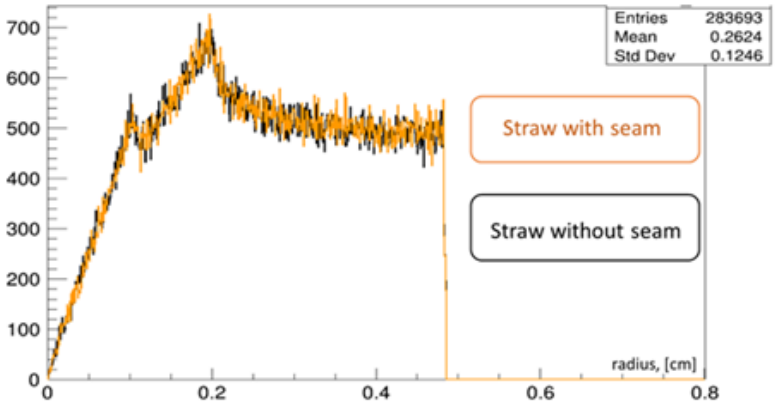

Fig. 52. Number of primary ionization electrons arriving to the anode from different distance. Garfield++.

But the arrival of electrons will be different in time, see on Fig. 53.

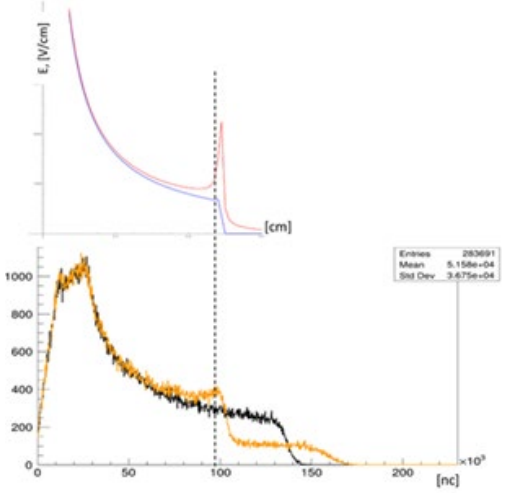

Fig. 53. Time of primary ionization electrons arriving to the anode from different distance Garfield++.

The simplify model of electron drifting in the straw tube

Motivation:

1. The main reason: after simulation of the drift of electrons inside the straw tube and analysis of the results obtained, it was concluded that Garfield++ does not take fully into account the mutual arrangement of the electric and magnetic fields for the COMET experiment. To test this hypothesis, a "toy model" of three-dimensional electron drift in a gas was built.
2. The motion of an electron in a straw tube is not flat. Garfield ++ and Garfield allows us to solve a flat problem.
3. Three-dimensional dependence of electron motion does not lose information about the Z axis. In this case, the isochronous map contains more accurate information about the electron drift time in the volume of the straw tube.

The implementation of the algorithm is shown in the Fig. 54.

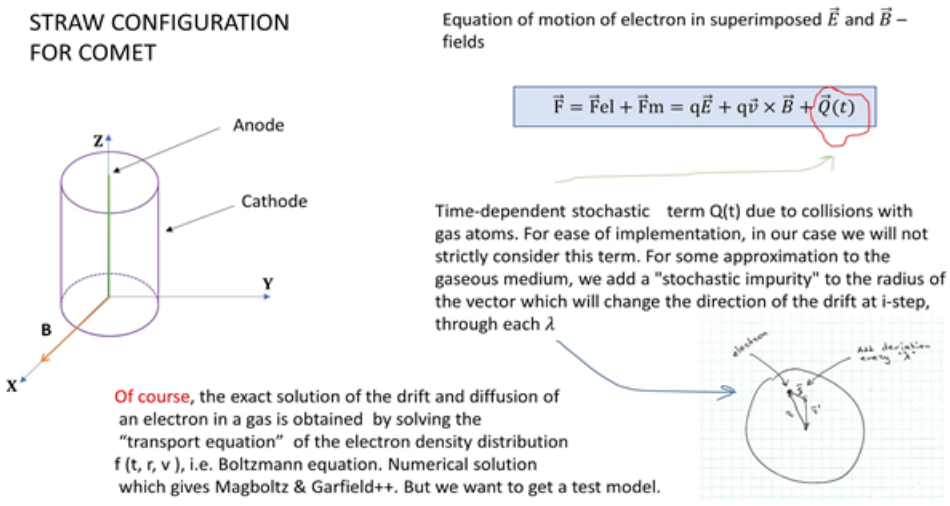

Fig. 54. The implementation of the algorithm for the three-dimensional electron drift in gas.

The above algorithm does not give accurate quantitative estimates of the motion of an electron in a gas, but gives a picture of the motion of an electron see Fig. 55.

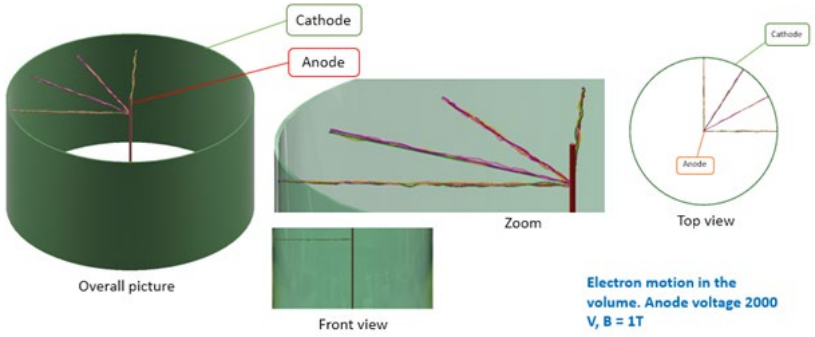

Fig. 55. Qualitative picture of electron drift inside the straw tube.

For example, select the following mixture of gases Ar-CO_2 (70-30). Also based on the previously given diffusion coefficient graph, it is possible to choose a lambda such that the XT ratios will practically coincide (Fig. 56).

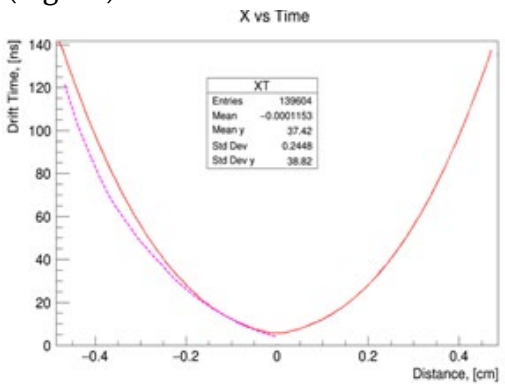

Fig. 56. XT relation custom equation (- - -) & Garfield++ Analytic field (—) Ar-CO_2 (70-30). Anode voltage 2000 V, B = 1T

As you can see, the proposed algorithm gives a more “fast” gas mixture. This is due, to the fact that the equation does not cover all the internal processes of electron drift in a gaseous medium. The artificial choice of the lambda coefficient contains an error.

From the distribution obtained, it follows that the electron trajectory can be considered as a straight line (Fig. 57).

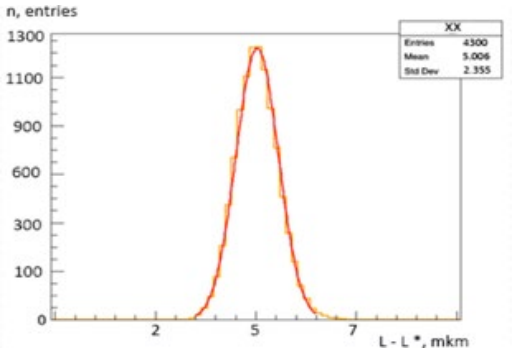

Fig. 57. The histogram of the difference between the real electron drift trajectory and the straight line. L - The path length of the electron in a gaseous medium. L* - The path length of the electron in a vacuum. Straight line.

The deviation of the drift lines from the straight line is on average 7 μm, which for the straw tube with a diameter of 9.75 mm is about 1/1000. Therefore, in this approximation, one can consider electron drift as a straight line.

2.3. Cosmic Ray Veto system

The COMET experiment plans to achieve the single-event sensitivity up to 10^{-17} for a single-event in coherent, neutrino-less μ → e conversion in the presence of an aluminum nucleus. It is necessary to exclude from the analysis data that may contain a trace from cosmic muons to ensure required accuracy. To fulfill this task, it is necessary to ensure the cosmic muons registration efficiency by the CRV (Cosmic Ray Veto) system at a level of 99.99% value.

The CRV system at COMET experiment is consists of two main parts. To establish required efficiency at front area, where the neutrons fluence is very high, the GRPC chambers is proposed to use. The module with scintillator strips in (SCRV) is proposed to use in other areas of COMET. Each SCRV module consist of 4 layers of scintillator strips sliced with aluminum sheets. Each layer consists of 15 strips. The WLS fibers are glued into the grooves at strips, and the light from the WLS fiber is collected by SiPM/MPPC photodetectors.

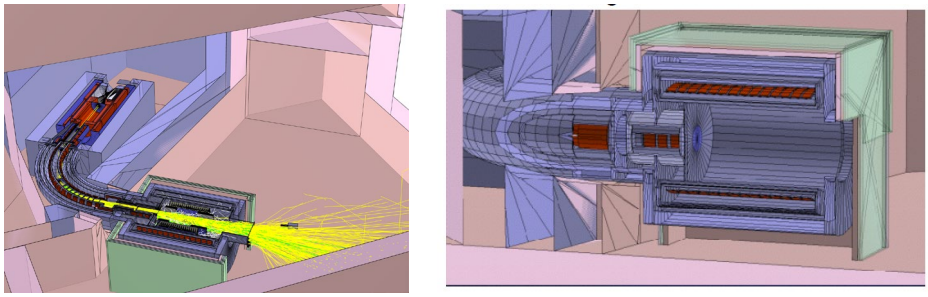

Fig. 58. COMET facility, phase 1. The detectors, colored by green correspond to CRV system.

We proposed design of the SCRV system, and the design for the central region of the SCRV system was approved by COMET collaboration.

To establish the optimal strip design, we conducted studies with various strip designs. To provide such studies, we purchased 1-m-length strips but various geometries: with a cross-section of 7x40 mm and 7x50 mm with two fibers, as well as strips with a cross-section of 7x160 mm equipped with eight fibers with a pitch of 20 mm. The cosmic muons registration efficiency was also simulated with GEANT4 for modules with various design.

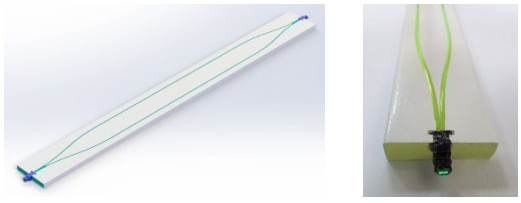

Fig. 59. Design of the strips with two WLS fiber.

To understand the influence of the gap between the working volumes of the adjacent strips, we studied the cosmic muon registration efficiency for modules with strips with different coatings, but the same geometry: 7x40 mm in cross-section and one

Kuraray Y11 (200) 1.2 mm WLS fiber for collecting light using SiPM Hamamatsu S13360-1350CS.

The 2-mm-thick steel sheets each painted with acrylic paint pigmented with TiO2 were placed between the layers. Various modules with 4x4 strip geometry were created. These modules were equipped with the same set of SiPMs during measurements.

A 4x4 module of 4x70 mm strips with one WLS fiber and a schematic arrangement of external counters to provide an independent trigger is shown on the Fig. 60.

This figure also shows histograms of the distribution from cosmic muons. Herewith, for those strips uncovered on the sides, a mean value of 20 ph.e. was observed, for the covered with AL-mylar – 21 ph.e. Also, an interesting relation found by experiment was observed for the module inefficiency and for each layer's multiplicities once it's fired for the uncoated at strips sides cases (red lines) in comparison with case when aluminized mylar is attached to the sides of the strip (blue lines).

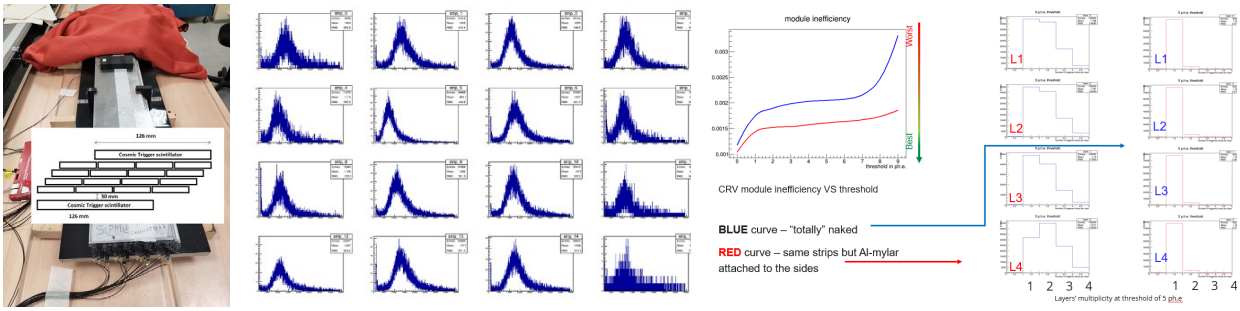

Fig. 60. Study of modules on cosmic muons: just the module; histograms for distributions of cosmic muons; the experimentally observed dependence of inefficiency by the threshold value for a module of 4x70 mm strips with one fiber, and the multiplicity of each layer once triggered.

The transverse scans using Sr^{90}/Y^{90} radioactive source of beta-particles were also performed in an aim to provide the necessary parameters for simulation according to a simplified scheme. The electron beam was confined by a 1-mm aluminum collimator.

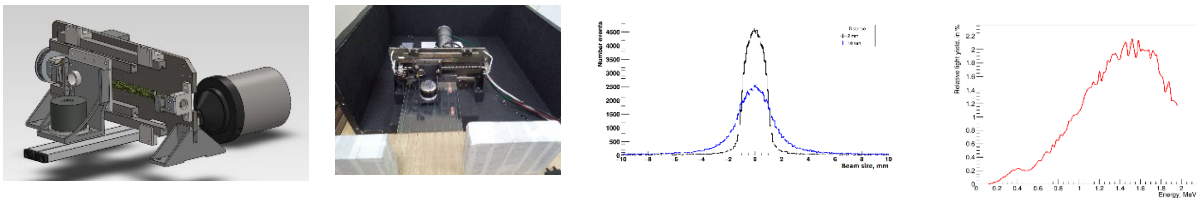

Fig. 61. Installation for the transverse scan using 1-mm-collimated beam of beta-particles from Sr^{90}/Y^{90} source.

Strips of various design were scanned in transverse direction. The strips with 7x40 mm in cross-section and with one WLS fiber were studies at first; then the strips with 7x40 mm and two WLS fibers and only side of strips covered my Al-mylar; strips with 7x160 mm in cross-section and 8 WLS fiber with step 20 mm between fiber also.

We also performed the transverse scan for the strips with 7x50 mm in cross section and two WLS fibers in in next options: strips had no cover; strips were side covered only; and strips fully wrapped.

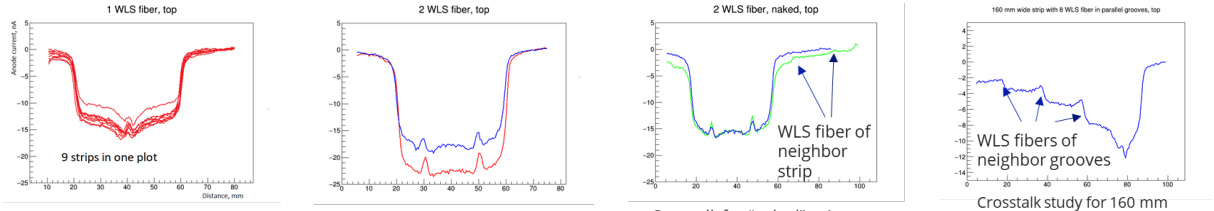

Summary plot for transverse scan for 9 strips with 1 WLS fiber (Al-mylar is attached to sides)

Totally "naked" strip
Same, but Al-mylar is attached to sides

Crosstalk for "naked" strips
blue – alone
Green – two strips side by side

Crosstalk study for 160 mm wide strip.
An influence from WLS fibers in neighbor grooves is visible

Fig. 62. The results of the transverse scan for the strips with 7x40 mm and 7x160 in cross section.

We also performed the transverse scan for the strips with 7x50 mm in cross section and two WLS fibers in in next options: strips had no cover; strips were side covered only; and strips fully wrapped.

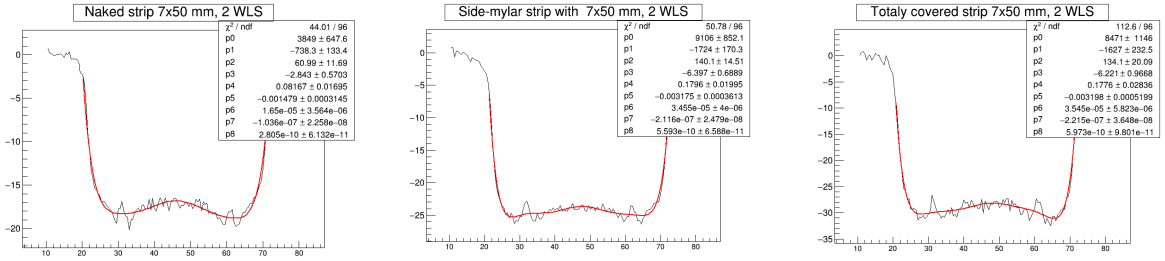

Fig. 63. The results of the transverse scan for the strips with 7x50 mm in cross section.

Observed The results observed by transverse scan allow us to perform the simulation of CRV module efficiency with GEANT4 for different strips design. Each layer of scintillation strips is shifted relatively to next by 9-7-7 pattern. Unequivocally clear that it is preferable to use strips with a width of 50 mm.

Aluminum sheets thikness	Efficiency for the module with 40-mm wide strip and pattern 9-7-7		Efficiency for the module with 50-mm wide strip and pattern 9-7-7		Comment:
	For 21 ph.e.	For 25 ph.e	For 21 ph.e.	For 25 ph.e	
2	0.9998 95	0.9999 92	0.9999 24	0.9999 99	Gap between neighbor strips set to 100 micron for all cases
10	0.9996 22	0.9999 25	0.9998 67	0.9999 81	

Table 3. Comparison of the muon registration efficiency for modules composed of the strips with a cross section of 7x40 mm and 7x50 mm. Both are equipped with two fibers.

Past year study of CRV module efficiency (both experimental and simulation) for modules with the standard technology of strips production, scilicet the creation of a reflective surface by creating, which creates gaps between the working volumes of adjacent strips of about 500 microns, showed that it is very difficult to achieve the required efficiency, 99.99% at a distance of 2.5 meters from the photodetector and needs to be improved. One of the ways to increase efficiency is to reduce the distance between the working volumes of adjacent strips. Changing the strips production in a way by the replacement of the side etching with mylar cover will reduce this gap from 500 microns to 130 microns. The width distribution for a bunch of 16 strips was also studied to evaluate the spread of widths during mass production of strips.

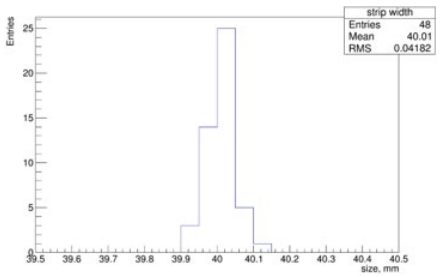

Layer of 16 strips	Width, mm	Gap between scintillating volumes	Technological gap, mm
Totally "naked" strip	640.5	0.033 mm	0.033 mm
same strips but Al-mylar attached to the sides	642.0	0.133 mm	0.033 mm

Fig. 64. The width distribution study for a bunch of 16 strips.

We also performed simulations with GEANT4 to select the optimal thickness of aluminum plates which should separate the scintillator strips layers to reduce background rates. We simulated different thicknesses of aluminum plates placed between layers, as well as rates layer by layer. The main result that was obtained by this simulation was that the basement layer should be at least 10-mm thick, and the intermediate layers should be 5-mm thick each in optimal case. In addition, in order to reduce the electron flux, it is necessary to place an additional shield consisting of a 10-mm thick HDPC block with 30% of Boron dopant and a 5 mm pure lead plate in front of the module.

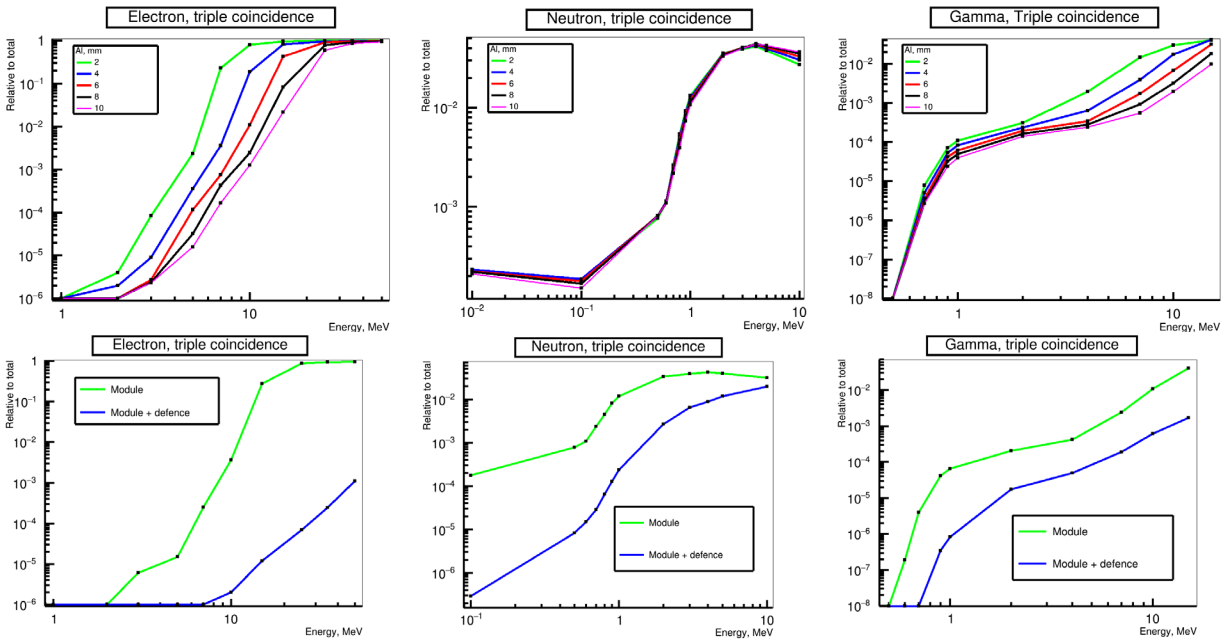

Fig. 65. Dependence of the rate for triple coincidences for electrons, neutrons, and gamma particles on the thickness of aluminum platinum (upper row, without any additional protection). Lower row: the rate comparison for 10-5-5-5-2 mm Al-sheet pattern based with protection (blue curves) against to same pattern module but no protection (green curve).

The obtained results allow us to propose to COMET collaboration the next, improved version of the CRV module based on 50-mm-wide and 7-mm-thick strips with 2 WLS fibers and the 10-mm Al-sheet as basement and 5-mm Al sheet to slices the CRV layers (10-5-5-5-2 pattern).

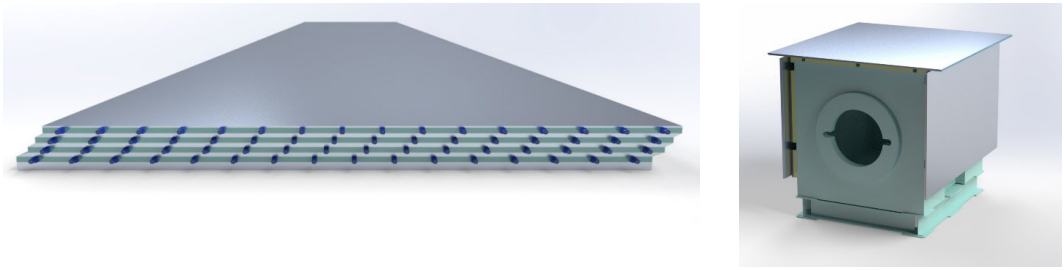

Fig. 66. CRV module design and its location on COMET installation for central region.

We also proposed the design of the fastening system for CRV modules and the auxiliary equipment to mount these CRV modules onto COMET installation.

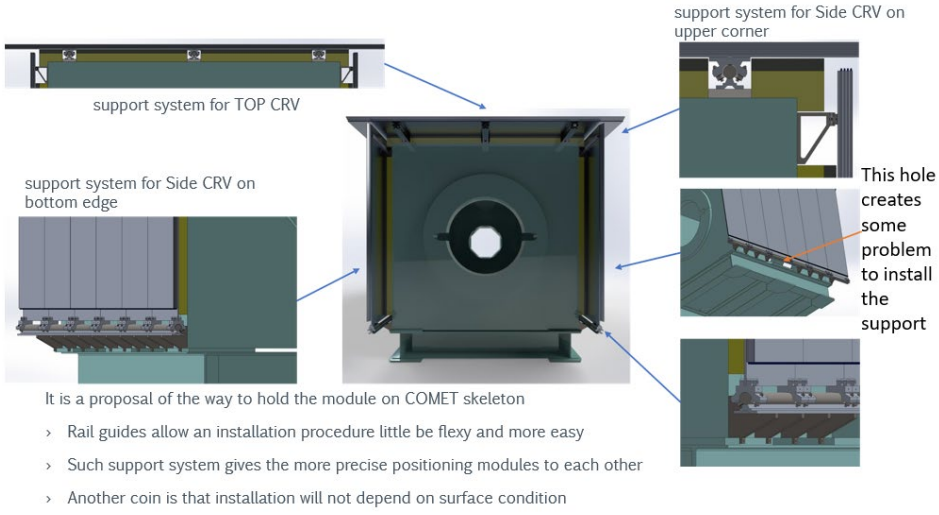

Fig. 67. The proposal of the CRV modules fastening system for central region of COMET installation.

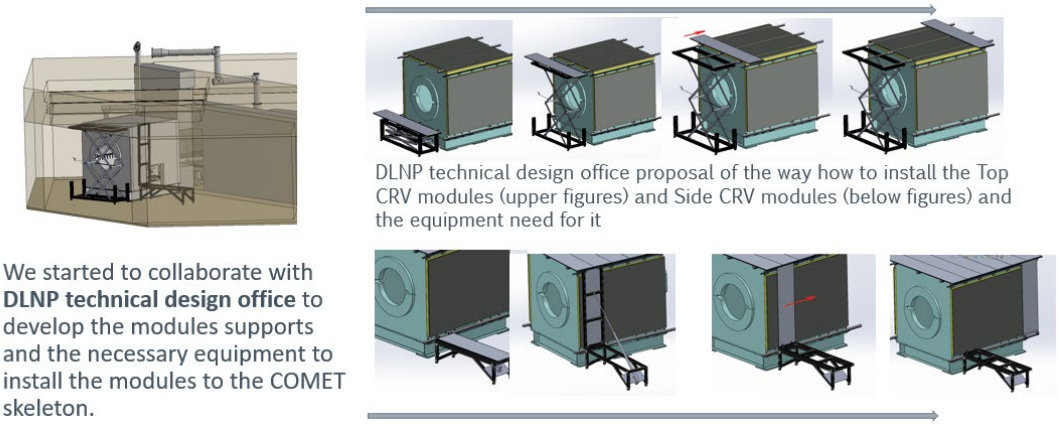

Fig. 68. Very first design of the auxiliary equipment to mount the CRV modules onto COMET installation.

We also initiated the design and already prototyped 32-channel Front-End electronics to get the data from photodetectors. To begin with, we explored the capabilities of the CitiROC ASIC chip, in order then to extend the experience gained onto a modern PetiROC chip. The double-pulse resolution is found no worse than 31 ns, even with the next signal lying on the tail of the previous one.

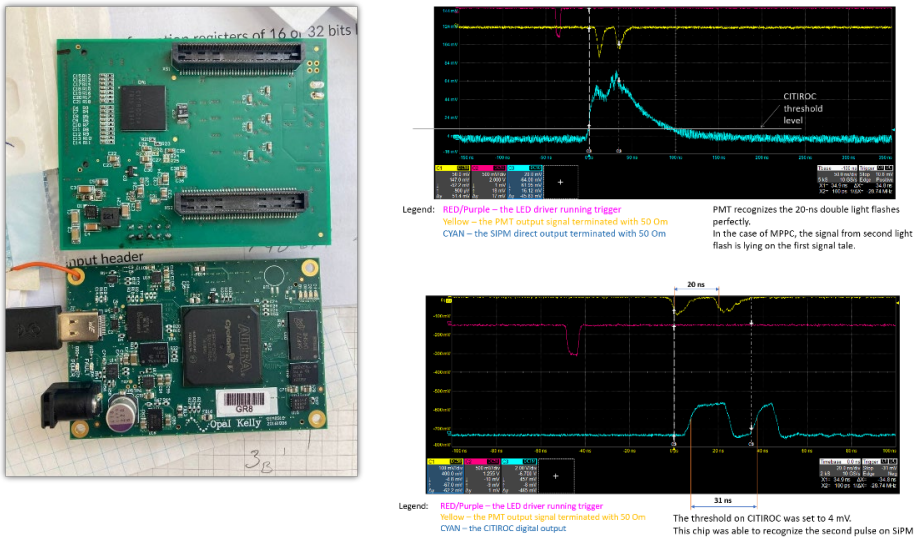

Fig. 69. The DAQ based on CitiROC fully designed by COMET-JINR team. Observing the double-pulse resolution.

To provide the quality test while its mass production time, we initiated to design of the corresponding test stand. The flat table with 6x1.2 m in surface was crafted. The 2D translation stage is installed on the table, which allows us to provide the quality check measurements with beta-source for 16 strips in one bunch. The possibility to use the front-end-electronics based on CitiROC for DAQ of quality test stand has been shown.

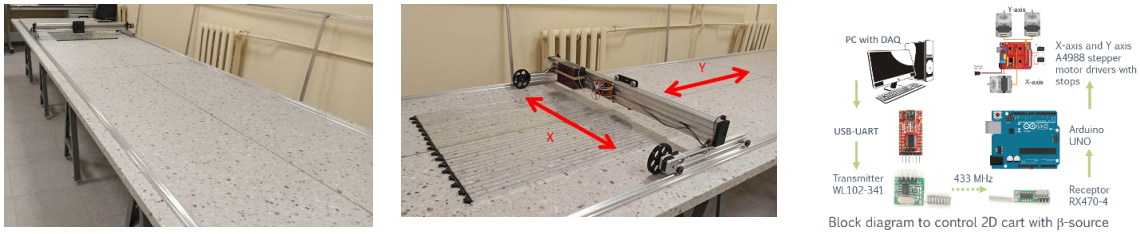

Fig. 70. The table with 2D translation stage on it. This stage has autonomous power supply and is controlled via WiFi.

We designed and built the first COMET CRV subsystem module, so called SCRV-LS-0, consisting of 4 layers of scintillation strips, 16 strips in each layer, with aluminum sheets separating these layers to reduce the effect of background events in conditions of being under high radiation (with fluence up to 1011 n/cm2 and the same for gamma for 100 days). To achieve this result, many studies have been carried out in terms of optimizing the light collected from the strip, also was needed to refine the geometry of the strip and to see the effect by increasing numbers of optical fibers. We ran simulations with GEANT-4 to find the optimal thickness of the aluminum sheets separating the layers of the module, also we needed to find the correct pitch to align the layers in relation to each other. A simplified method for determining light collection from a strip was developed to optimize simulation time. The issue of selecting a radiation-resistant optical glue was also investigated, as well as the selection of an appropriate adhesive mixture for gluing layers and its subsequent check to ensure that light

collection does not decrease during gluing, while the mechanical characteristics of the gluing area should remain at the required level (no worse than 300 kPa shear stress).

To create this first module, we developed and improved then the appropriate technology to produce strips, as well as a procedure for quick check of the quality for WLS fibers. After manufacturing the strips, it is also required to check their quality. For this, a special table 6x1.2 meters was created with a lightproof box over the entire surface and a radio-controlled 2D portal inside. A technique for checking the quality of strips using this table was developed.

The module itself was also tested and then assembled/glued by using vacuum to create the necessary pressure of 1 kg/cm^2 to ensure proper fixation of the module parts during the curing of the adhesive.

Once the module was assembled, its first tests are scheduled with the proper electronics to detect cosmic muons. Also, this module should be sent to Japan so that it can be studied during the COMET-alpha phase. Based on the results achieved, a decision will be made on the next serial production of these modules, as well as on the production of the electronics attached to them.

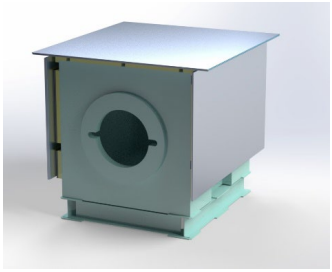

Fig. 71. An approximate location of our developed SCRV Top, Left, Right subsystems on the COMET facility. Subsystems SCRV Back, GRPC-CRV are not shown.

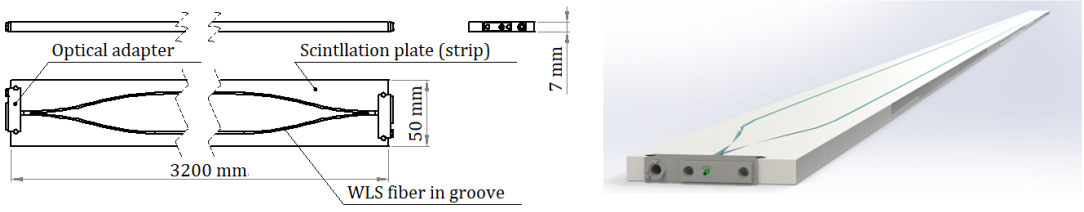

Fig. 72. Strips design.

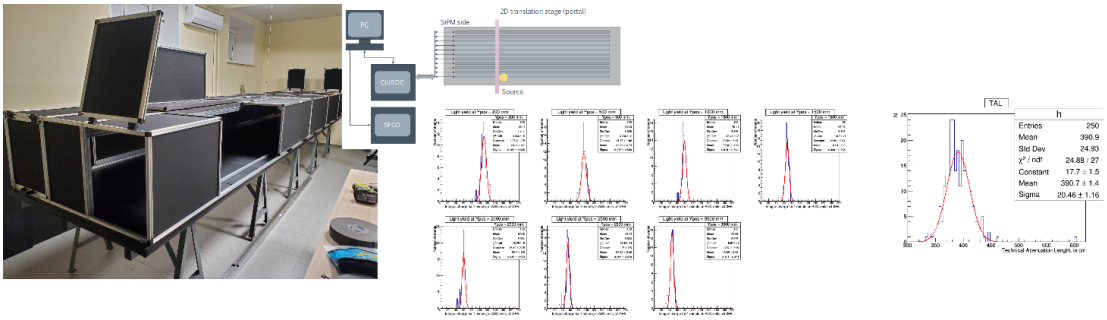

Fig. 73. Table to test strips parameters. Diagram of the DAQ. Results.

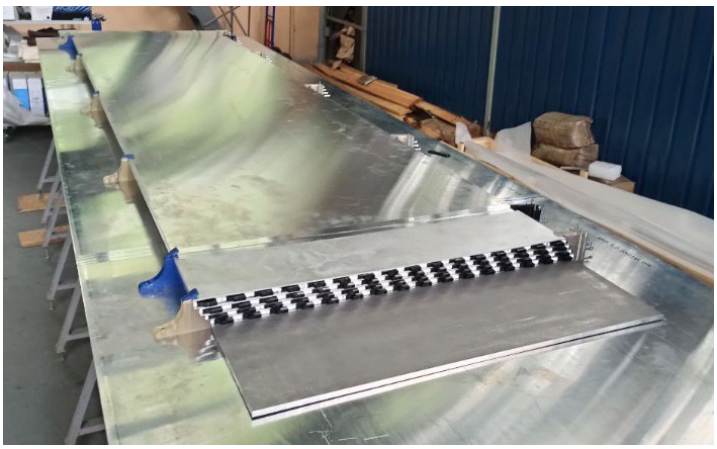

Fig. 74. Created at JINR SCRV-LS-0 module for COMET experiment.

These results were discussed inside on regular collaboration and CRV team meetings, also were reported on COMET Collaboration meetings CM33, CM34 и CM35. Several publications in the refereed literature describing these studies are also in schedule.

2.4. Simulation and Data Analysis

Development of the straw tracker and calorimeter systems required a lot of simulation work. The corresponding results are presented in the Technical Design Report for Phase-I of COMET. In particular, the values of efficiency and space resolution in different conditions: for the tubes of different diameters, wall thicknesses and gaps between the tubes, for the straw tracker have been established. Similarly, the calorimeter simulation has been done for two types of crystals, GSO and LYSO using the real optical parameters. Among others, simulation of light outputs and light collection with different reflecting materials also has been performed. Simulated energy resolution was found to be better for the LYSO type what has been confirmed later experimentally.

A dedicated simulation has been done with the aim to optimize the operation of the J-PARC Main Ring in order to achieve very low extinction factor, below 10^{-9}, what is the crucial point for the COMET.

A very essential task is working in the COMET software - ICEDUST (Integrated Comet Experimental Data User Software Toolkit), in particular, to simulate the response of the straw tracker in ISEDUST.

The Geant4 simulation of the optimal structure of the segmented calorimeter for the COMET experiment was made. The simulation of the electromagnetic calorimeter was included in the framework ICEDUST, which is adopted framework for any COMET software activity.

The data from the calorimeter prototype beam test has been analyzed independently in Japan, based on the similar analysis. Both analyses have led to the conclusion about a better performance of the LYSO crystals.

Since the optical model of LYSO crystal is not implemented in the GEANT4, an optical model of LYSO crystal was developed. To obtain the optical model of the crystal, the SLitrani

package and measurements of the main optical parameters of the crystal performed on the setup were used. To verify the G4 optical model, G4 simulation of LYSO crystal was performed.

The simulation of the optimal structure of the ECAL calorimeter was performed based on the Geant4 package by using the optical model of LYSO crystal. The simulations were made taking into account the real conditions of the COMET experiment: 1) the calorimeter was located in 1 T uniform magnetic field; 2) electron beam energy spread was 105 ± 0.5 MeV, and beam spot was 1 cm^2 ± 1 cm; 3) the crystals were wrapped with two layers of Teflon (thickness 60 μm). These simulation conditions are similar to the conditions under which it was performed Beam Test in Tohoku (except the magnetic field) of calorimeter prototype for LYSO and GSO crystals. Thus, the obtained Geant4 optical model can be used to simulate the calorimeter and for data handling of the COMET experiment.

In the future, we are planning to enlarge our scope of works on simulation and analysis in order to be ready for a physic analysis for the COMET data from J-PARC.

3. Summary

- The first stage of the COMET program will provide an opportunity to fully understand the novel superconducting pion production system and muon beam line, with its charge-and-momentum selecting dipole fields which are superimposed on the curved solenoids which form the pion and muon transport section - a design that is unique to COMET amongst intense pulsed muon beam facilities.
- The research program for Phase-I encompasses both a search for muon-to-electron conversion with a sensitivity that is about 100 times better than the current limit, and a dedicated detector set-up, which will allow us to make comprehensive measurements of the muon beam.
- Detailed rate and timing studies and other measurements from Phase-I will help us understand the backgrounds to the muon-to-electron conversion measurement. These will be crucial as COMET prepares to move to Phase-II, which is to improve the sensitivity by another two orders of magnitude.
- The challenges to building and running this high-background rare-decay search experiment are addressed, including: proton and muon beam dynamics; the superconducting magnet systems; high-rate data-acquisition systems; operation in harsh radiation environments; software and computing systems that can meet the demands of the experiment.
- The COMET Collaboration believes that rapid execution of Phase-I, which will consist of data taking in numerous different configurations of the beam line and detector systems, to be followed by the deployment of Phase-II soon after, is the most reliable path to a high-sensitivity search for $\mu^- \longrightarrow e^-$ conversion. The program has the potential to result in a paradigm-shifting discovery, which could lead to an entirely new field opening up of multiple measurements of different charged-lepton flavour violating processes, a new era of discovery in particle physics.
- The role of JINR in the COMET experiment is quite visible and recognized by the COMET Collaboration.

4. The responsibility of the JINR in the COMET

- The JINR group is a single one in the COMET collaboration, which is capable of producing thin-wall straw tubes. Therefore, we are fully responsible for manufacturing all straw tubes. Different procedures of the tube tests on pressure, gas leakage and elongation have been also updated in accordance with the COMET requirements and new test standards have been established.
- JINR takes full responsibility for the next step to this direction, carrying out of R&D works of straw tubes for the COMET Phase-II, with the tubes of 5 mm diameter and 12μ wall thickness. For this purpose, we are preparing a new straw line in DLNP.
- JINR physicists together with the KEK colleagues take full responsibility in assembling, tests and installation of the full-scale straw tracker for Phase-I. Appreciating the crucial contribution of the JINR to the creation of the straw tracker, a member of JINR-COMET team was elected as one of the coordinators for the straw tracker system.
- JINR proposed the idea and took full responsibility in production of a full-scale straw station for Phase-I, with new types of straw tubes.
- JINR takes full responsibility for development and optimization of a crystal calibration method for the calorimeter to be used in COMET Phase I and Phase-II.
- JINR together with KEK and Kyushu University takes full responsibility for assembling, testing, installation and operation of the calorimeter.
- Physicists from JINR take full responsibility for the certification of crystals, and are the leaders in the R&D work.
- JINR physicists have implemented a full-scale R&D program to create a cosmic veto system. The program was completed successfully, and the results were reported at the collaboration meetings. Based on these results, all the parameters and methods for creating the CRV are determined. Also, the main responsibility in the assembly, testing and installation of the CRV for Phase-I will be on scientists from JINR. Based on these, a member from the JINR group was elected as the COMET-CRV leader.

5. Further plans foresee

- Participation in the preparation, engineering and physics run, the data acquisition and analysis of Phase-I, 2024-2026
- R&D program for production of the straw tubes of 12 μm wall thickness and 5 mm diameter. Measuring of all mechanical properties and development of standards for quality control of manufactured of the 5 mm brand-new straw tubes, 2024 -2025
- Finalization assembling, testing, calibration, installation, cosmic test and maintenance of the straw detector for Phase-I, 2024
- Production of straw tubes (about 1000 pcs) for full-scale prototype, 2024-2025
- Production of a full-scale straw station in JINR, with new tubes (12 μm, 5 mm), and measurements on the beam, 2024-2025
- Preparation and mass-production and testing of straw tubes for Phase-II, 2025-2026

- Development and optimization of a crystal calibration method for a COMET calorimeter, given the features of the experiment: the presence of a magnetic field and high-resolution calorimeter, 2024-2026
- Participation in the full calorimeter designing, assembling, installation, cosmic test and maintenance, 2024-2026
- Participation in the assembly and maintenance of the CRV for Phase-II, 2024-2026
- Participation in the beam tests of the detector components for Phase II, 2025-2026
- Participation in assembling, testing, installation and maintenance of whole detector system for Phase-II, 2025-2026
- Complex detector system (tracker, calorimeter, etc.) simulation, 2024-2026
- Participation in the engineering and physics run for Phase I, 2024-2025
- Participation in the data acquisition and analysis, 2025-2026

6. Manpower

No.	Full name	Division	Position	Amount of FTE
1.	D. Aznabaev	BLTP	Researcher	0,3
2.	D. Baigarashev	VBLHEP	Researcher	0,4
3.	A. Boikov	DLNP	Junior researcher	0.3
4.	D. Chokheli	DLNP	Senior researcher	1.0
5.	T.L. Enik	VBLHEP	Senior researcher	0.3
6.	D. Goderidze	MLIT	Junior researcher	0.5
7.	P.G. Evtukhovich	DLNP	Senior researcher	1.0
8.	A. Issadikov	BLTP	Senior researcher	0.3
9.	V.A. Kalinnikov	DLNP	Leading researcher	1.0
10.	A. Khvedelidze	MLIT	Leading researcher	0.4
11.	G.A. Kozlov	BLTP	Leading researcher	0.3
12.	A.V. Pavlov	DLNP	Junior researcher	1.0
13.	B.M. Sabirov	DLNP	Researcher	1.0
14.	A.V. Simonenko	DLNP	Senior researcher	1.0
15.	V.V. Tereshchenko	DLNP	Group Leader	0.3
16.	Z. Tsamalaidze	DLNP	Head of the Sector	0,7
17.	N. Tsverava	DLNP	Junior researcher	1.0
18.	I.I. Vasiliev	DLNP	Junior research	0,3
19.	E.P. Velicheva	DLNP	Senior researcher	1.0
20.	A.D. Volkov	DLNP	Researcher	1.0
21.	I. Zimin	DLNP	Junior researcher	0.3
22.	I.L. Evtukhovich	DLNP	Senior engineer	0.9
23.	E.S. Kaneva	DLNP	Engineer	1.0
24.	X. Khubashvili	DLNP	Engineer	0.9
25.	A.G. Samartsev	DLNP	Senior Engineer	0.4
26.	S.V. Tereshchenko	DLNP	Engineer	0.5
	Total:			**17.1**

Project Leader Z. Tsamalaidze